Students/Young Researchers Poster Session

Risk-Consistent earthquake for regional disaster prevention planning

Minoru Matsubara, The University of Tokyo, JAPAN

Background

Probability should be considered

In Japan, each prefecture estimates loss on deterministic earthquake scenarios. Usually, scenarios used for the loss estimation has a very low probability of occurance, but cause very large loss if they occur (Point A in below Figure). Human lives are very important. So they must be protected even if extraordinary large earthquake occur. <u>But when considering continuation of economic activity, it costs too much to design trains or production facilities to endure Point A. it' s not reasonable.</u> In this case, Point B is more important than Point A because the former has a high probability of occurance .

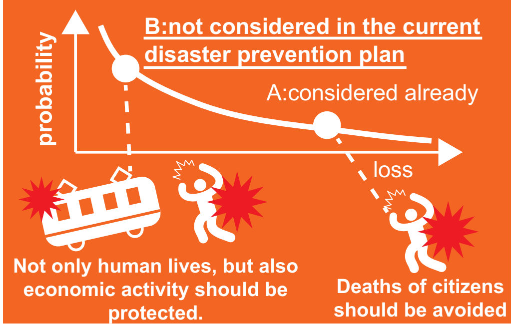

Aim Applying PSHA for identifying most probable earthquake

Weakpoint of PSHA

Probabilistic seismic hazard analysis (PSHA) shows us the relationship between the regional impact caused by future earthquakes (like deaths, collapse of structures) and its exceedance probability. this relationship represents all events, but when making a seismic prevention plan, a single "design earthquake" is often desired.

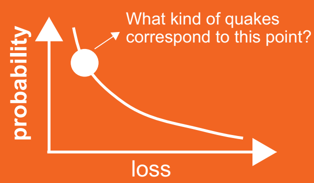

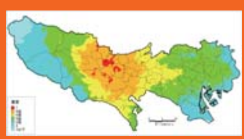

Proposed Method

In this study, using PSHA, a single "design earthquake" is made in steps shown in following figure.

1. Select some urban functions which you want to keep after disaster

2. Define the target probability in which each urban function should be protected.
3. From PEX*-prob. curve, caluculation the target PEX corresponding the target period defined above

*:PEX=" Population Exposed to Seismic Intensity" (mentioned below section)

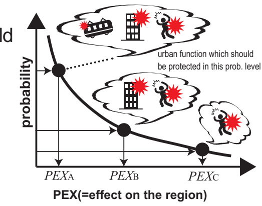

4. Find the Seismic zone which is most likely to exceed the target PEX

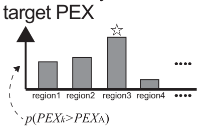

5. Find the parameter which is most likely to cause larger PEX than the target PEX in the region. From the found parameter, you can make a single "design earthquake" .

M, x, ε

Population Exposure to Seismic Intensity (PEX)

In this research, loss of an earthquake is represented by "Population Exposure to Seismic Intensity" (PEX) . PEX is calculated from distribution of population and that of seismic intensity (the figure on the right). PEX is a simple and clear index because it doesn' t depend on a complex hypothethis which is need to calculate loss

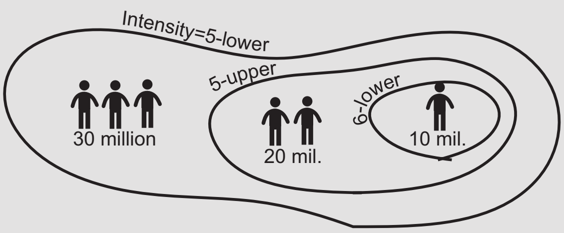

In above case...
PEX for the Seismic Intensity 5-lower = 60 mil.
PEX for the Seismic Intensity 5-upper = 30 mil.
PEX for the Seismic Intensity 6-lower = 10 mil.

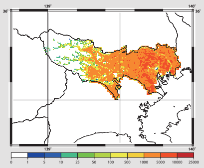

population distribution

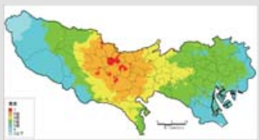

Seismic Intensity distribution

Result of Tokyo

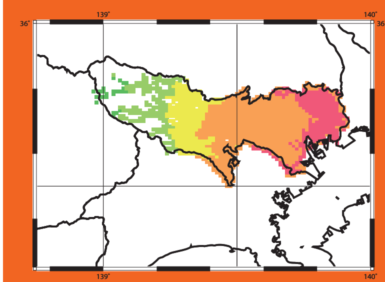

a "design earthquake" used for protection of economy activity

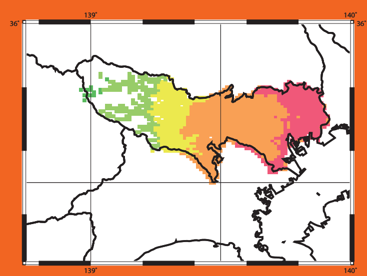

a "design earthquake" used for protection of structures

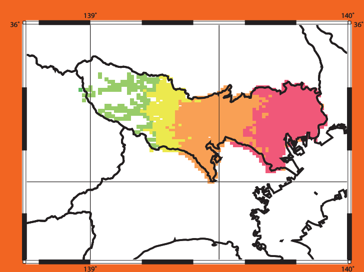

a "design earthquake" used for protection of human life

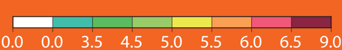

Seismic Intensity

Case Study of Tokyo prefecture

Seismic Zones

Below figures show earthquake models used for this study. **I** shows inland earthquake source faults specified by geological reserches or histrical record. **II** show source of subduction-zone earthquakes. **III** show models of earthquakes whose hypocenter and magnitude are not specified. Colors of **III** mean frequency of earthquake occurance.

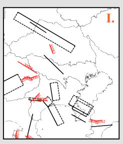

Specified Faults (inland)

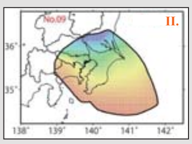

Kanto earthquake

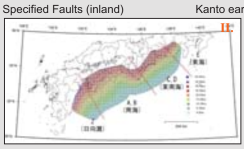

Nankai Trough earthquake

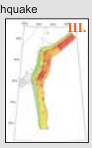

Pacific Plate earthquake

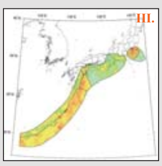

Philipin Sea Plate earthquake

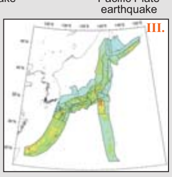

Inland earthquake

Pop. distribution

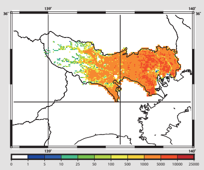

PEX-prob. curve

Colored lines correspond to each seismic zone' s result. Black line is a result which combines them all.

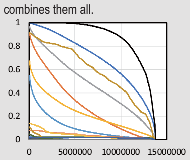

PEX for Seismic Intensity 5-upper

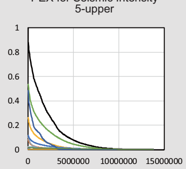

PEX for Seismic Intensity 6-upper

Urban function-prob. matrix

This matrix is based on values used in structural design (such as VISION 2000). Human lives are most important, so even if a very rare and large earthquake occur, they must be protected. On the other hand, when a frequent earthquake occur, economic activity should also be protected, not only human lives.

exceedance probability	function			loss
	economic	structures	human life	
63% in 50yr.	○	○	○	small
39% in 50yr.		○	○	midium
10% in 50yr.			○	large

○=function which should be protected

The Seismic Zone which is most likely to exceed the taget PEX

$$\text{contribution to the target } PEX \text{ of zone } k = \frac{P(PEX_k > PEX)}{\sum P(PEX_k > PEX)}$$

protection of economic activity	contribution
Nankai Trough Earthquake	0.37
Philipin Sea Plate quake	0.27
Pacific Sea Plate quake	0.23
protection of structures	**contribution**
Nankai Trough Earthquake	0.37
Philipin Sea Plate quake	0.24
Pacific Sea Plate quake	0.20
saving lives	**contribution**
Philipin Sea Plate quake	0.27
Pacific Sea Plate quake	0.26
Nankai Trough Earthquake	0.18

Estimation of the distribution shape of story stiffness using the structure dynamic properties identified from earthquake observation at two points

University of Tokyo
Takada Laboratory
Sangwon Lee

1.Introduction

Earthquake observation is generally carried out only on few stories of a building, due to its costly nature of setting up and running the sensors. For instance, if the only two points of a building are observed,

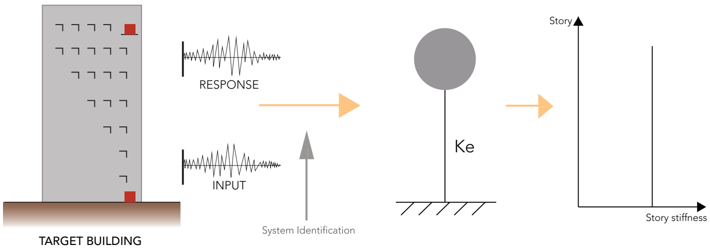

However, as it is hardly possible that every story get damaged equally , the story stiffness should be estimated by its distribution shape.

Drawbacks of past research

Some research estimate the response or damage of unobserved story by few points that are inspected. Actually, for that research being done, numerical analysis model or mode shapes are needed. However, numerical analysis model or mode shapes are required for those research and thus, it may fail to take account of the mode shapes which are changeable factors related to damage and time. If we can estimate the distribution shape of the store stiffness without establishing the mode shapes, it will be far more practical and reasonable method for detecting damage.

Purpose of the current research

Based on these things,
(1) Proposal of the estimating method of story stiffness distribution shape with 2 following conditions.
1. Without mode shape and analysis model
2. Using the 2 observation points (top and bottom floor)

(2) Verification of the suggested method by the response analysis of the rocking model as well as base-fixed model.

2. Proposal of Estimation Method

The inverse eigenvalue problem

The eigenvalue problem of MDOF structure can be expressed as follows.

$$|[K]-\omega^2[M]|=0$$

The stiffness matrix can be derived by putting the some cases that..
(1)The Identified vibration modes are dominant.
(2)Mass matrix is already known (supposing from floor plan).
(3)No sudden changes exist on the distribution shape of story stiffness.

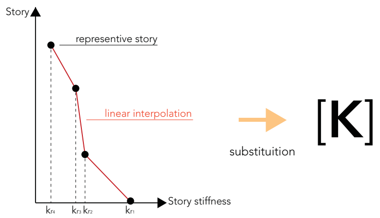

(Step1) Select the representive stories.
(Step2) Connect the representive stories with a straight line on the story stiffness plot.
(Step3) Fill in the stiffness matrix with the Eqs expressed by representative story stiffness.
-> As the number of Eqs and of values are same, the values can be found.

The sequences of estimation

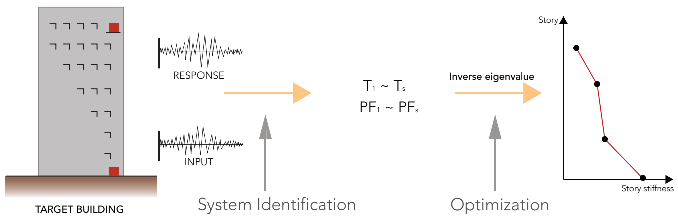

System Identification Optimization

Suggestion of optimization algorithm

The basic rule is to select the distribution shape which has the smallest error.
When we consider the identified natural periods, the error function is expressed by Eq.(2).
Eq.(3) is used for considering the participation functions along with the natural periods

$$\mathrm{Error}=\sum_{s=1}^{4}(T_s-T_s')^2 \quad (2)$$
$$\mathrm{Error}=\sum_{s=1}^{4}\{(T_s-T_s')^2+(\beta_s\phi_s-\beta_s'\phi_s')^2/\eta\} \quad (3)$$

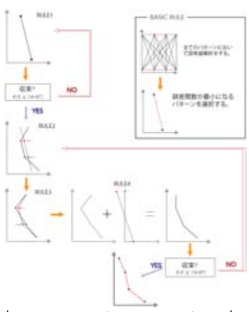

For rocking of the base,
Add Stiffness matrix to rotational spring value, and mass matrix to rotational inertia.
Consider the rotational spring value as a variable to Overall steps of algorithm.

3. Verification

Verification of optimization algorithm

Verify the suggested optimization algorithm when natural periods and mass matrix are known.

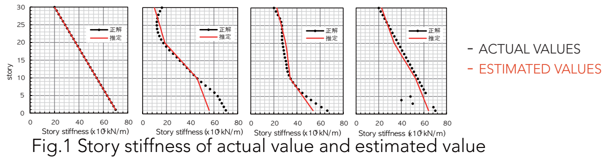

Fig.1 Story stiffness of actual value and estimated value

If the mass matrix and natural periods are known, by using the suggested algorithm, it is possible to estimate approximate shape of story stiffness distributions.

Verification by linear response analysis using fixed base model

Table.2 Natural periods & Participation function

	T_1(s)	T_2(s)	T_3(s)	T_4(s)	$\beta_1\phi_1$	$\beta_2\phi_2$	$\beta_3\phi_3$	$\beta_4\phi_4$
Set value	2.18	0.76	0.47	0.34	1.31	-0.50	0.33	-0.24
ID	2.18	0.77	0.47	0.33	-	-	-	-
Estimation	2.18	0.78	0.47	0.34	1.32	-0.51	0.32	-0.22

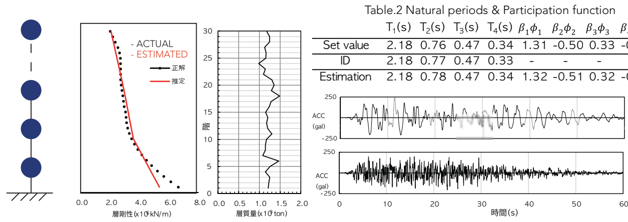

Fig.2 story stiffness Fig.3 mass Fig.4 Time history of input & ouput wave

Estimation method for rocking model

Real buildings are rarely considered by fixed base. It is often pointed out that the rocking base strongly influence lower mode(especially 1st mode). By the response analysis using rocking model, the validity of the suggested method would be certified by assuming 3 cases.

Table. 1 verification cases

	Assuming model	Considering dynamic properties
Case1	Fixed base	1~4 thnatural period
Case2	Rocking	1~4th natural period
Case3	rocking	1~4thnatural period& participation function

Verification by linear response analysis using rocking model

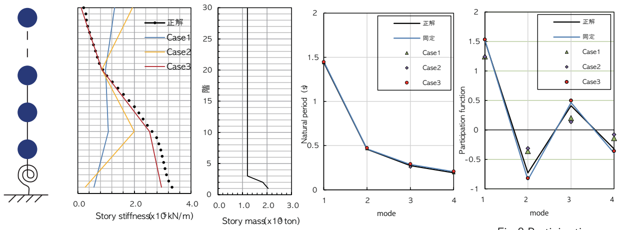

Fig.5 Story stiffness distribution shape Fig.6 Story mass distribution shape Fig.7 Natural period Fig.8 Participation function

4. Conclusion

1) If low-order natural periods are found、by suggested method、stiffness distribution shape can be estimated within practical ranges.
2) By the suggested method using only lower order dynamic properties、estimating localized damages is approximately possible
3) If fixed base is established、stiffness can be estimated in some measure by using only natural periods (case1)
4) If base locking has a great effect、considering low-order natural periods and participation functions, story stiffness can be estimated by high accuracy(case3)

Statistical Analysis of Site-Specific Ground Motion Prediction Based on Hierarchical Bayesian Model

T. Hamada[1], T. Itoi[2] , N. Sekimura[3]

[1] Master student, Graduate School of Engineering, The University of Tokyo, Tokyo, Japan, hamada@safety.n.t.u-tokyo.ac.jp

[2] Associate Professor, Graduate School of Engineering, The University of Tokyo, Tokyo, Japan, itoi@n.t.u-tokyo.ac.jp

[3] Professor, Graduate School of Engineering, The University of Tokyo, Tokyo, Japan, sekimura@n.t.u-tokyo.ac.jp

Introduction

Probabilistic Seismic Hazard Assessment(PSHA)

- The main objective of PSHA is to establish a design ground motion and to assess risks of potential accidents.
- PSHA aims to quantify of future ground motion uncertainties that consist of location, magnitude, occurrence, and ground motion prediction.
- This study mainly focuses on uncertainty associated with the ground motion prediction.

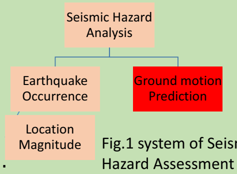

Fig.1 system of Seismic Hazard Assessment

Ground motion prediction

- Attenuation relationship is a regression of the observed ground motion data based on Site-to-fault Distance(X), Moment Magnitude(Mw), and average shear-wave velocity to 30m depth(V_{s30}).
- Conventionally, the least-square method is used in order to construct the attenuation relationship.
- But the least-square method assumes the ergodicity assumption that is widely used for seismology, simply defined as follows.

$$Average\ of\ time = Average\ of\ place$$

- This assumption sometimes causes biases in prediction.

Hierarchical Bayesian model

- Bayesian statistics provides a method for describing degree of belief using the mathematical language of probability. Bayesian statistical methods start with existing 'prior' beliefs, and update the beliefs using data to give 'posterior' beliefs, which may be used as the basis for inferential decisions.
- Bayes' theorem is described as follows

$$p(\theta|y) = \frac{p(y|\theta)p(\theta)}{p(y)} \qquad (1)$$

Where $p(\theta)$; $prior\ distribution$, $p(y|\theta)$; $likelihood\ distribution$ ($data\ distribution$), $p(y)$; $normalizing\ factor$.

- The above Bayes' theorem is extended to Hierarchical Model(Fig.2&3).

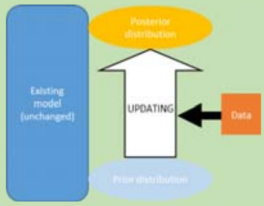

Fig.2 Overview of normal Bayesian Updating

- In order to include the site-specific characteristics, we introduce the individual terms.

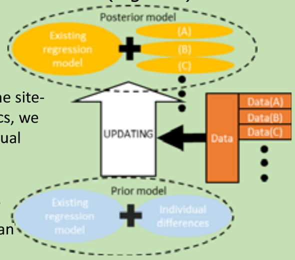

Fig.3 overview of Hierarchical Bayesian Updating

Statistical Analysis Method

Data set

- Observed records from crustal earthquakes at 571 sites (44 earthquakes, 1703 records) are used.

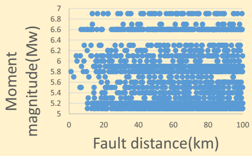

Fig.4 relation between Moment magnitude and Fault distance.

Regression Model

- Based on some previous study, the following equation is adopted

$$I = aMw - 2\log(X + b \times 10^{0.5M}) - cX + d + E + \varepsilon \qquad (2)$$

where I ; $ground\ motion\ intesity$, M ; $Moment\ Magnitude$, X; $fault - to - site\ distance$, E; $site - specific\ characteristics$, ε; $error\ term(0, \sigma^2)$ a, b, c, and d ; $regression\ coefficient$

Markov Chain Monte Carlo Method(MCMC)

- MCMC is an algorithms for sampling from a probability distribution based on constructing a Markov chain that has the desired distribution as its equilibrium distribution. In the Markov chain next sample depends on present realization as follows:

$$X^{(t+1)} \sim p_{trans}(x|X^{(t)} = x^{(t)}) \qquad (3)$$

Gibbs Sampling

- Gibbs sampling is one of the most widely used algorithms, for MCMC. This method generates a multi-dimensional Markov chain by splitting the vector of random θ into subvectors and sampling each subvector in turn, conditional on the most recent values of all other elements of θ.
- Sample a new value θ_1, from the full conditional distribution ofθ_1, given the most recent values of all other elements of θ as follows:

$$\theta_1^{(1)} \sim p(\theta_1|\theta_2^{(0)}, \theta_3^{(0)}, \ldots, \theta_k^{(0)}, y) \qquad (4)$$

Result and Conclusion

The result of least-square method

- Fig.4 shows the result of least-square method
- The equation on the below is derived from 3-step stratified least-square method.

$$I = 1.36Mw - 2log_{10}(X + 0.00550 \times 10^{0.5Mw}) - 0.00670X - 1.63log_{10}V_{s30} - 3.30 \qquad (5)$$

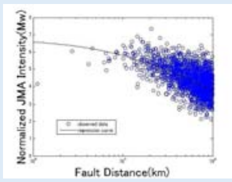

Fig.4 comparison between observed records and regression (least-square)

The result of Hierarchical Bayesian method

$$\begin{matrix} ground\ motion \\ predictions \\ for\ each\ site \end{matrix} = \overbrace{aM - 2\log(X + b \times 10^{0.5M}) - cX + d}^{existing\ attenuation\ relationship} + \overbrace{\vdots}^{site-specific\ term}$$

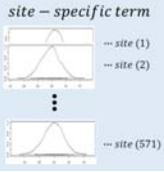

Fig.5 how to construct the ground motion prediction equation for each site

- Fig.6 shows the result of Hierarchical Bayesian method including site-specific terms
- The equation on the below is derived from Hierarchical Bayesian method which can estimate the standard deviation of each coefficient.

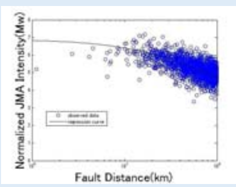

Fig.6 comparison between observed records and regression (Hierarchical Bayesian method)

$$I = 1.32(\pm 0.04)Mw - 2log_{10}(X + 0.00481(\pm 0.002) \times 10^{0.5Mw}) - 0.00427(\pm 0.0009)X + E - 0.786(\pm 0.2) \quad (\pm : error) \qquad (6)$$

Discussion on site-specific term

- Compared with least-square method(LSM) and Hierarchical Bayesian method(HBM), the standard deviation (σ) HBM is smaller than that of LSM.

	Least-square	Hierarchical Bayes'
σ	0.608	0.465

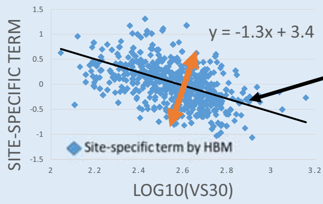

Fig.7 relation between site-specific term and Vs30m/s

- Fig.7 indicates that site-specific term corresponds to the characteristics of the site amplification.
- Standard deviation ; 0.356

- This approximate line is the ergodicity assumption (cf. 1.63 in Eq(5)).
- Compared with these standard deviations, equation on the below can be obtained

$$\sqrt{(0.465)^2 + (0.356)^2} = 0.586$$

- This result(0.586) comparable to the standard deviation of least-square method(0.608). The overestimation of σ is considered due to the ergodicity assumption in the LSM

Conclusion

- By employing the Hierarchical Bayesian Model, the site-specific attenuation relationship is developed by adding the site-specific term to the existing attenuation.
- As a result, compared to the standard deviation value of existing attenuation relationship(0.608), this method can reduce that value to 0.465.
- As a future work, the methodology for site-specific PSHA will be developed.

Ground motion prediction for estimating earthquake scenarios for SSCs in DiD Level 4

Y. Iita(1), T. Itoi(2), N. Sekimura(3)

(1) Master student, Graduate School of Engineering, The University of Tokyo, Tokyo, Japan, iita@safety.n.t.u-tokyo.ac.jp
(2) Associate Professor, Graduate School of Engineering, The University of Tokyo, Tokyo, Japan, itoi@n.t.u-tokyo.ac.jp
(3) Professor, Graduate School of Engineering, The University of Tokyo, Tokyo, Japan, sekimura@n.t.u-tokyo.ac.jp

東京大学 THE UNIVERSITY OF TOKYO

Introduction

One of lessons learned from the 2011 Great East Japan earthquake and the Fukushima Daiichi Nuclear Power Plant accident is importance of implementation of the defense in depth concept as countermeasures against external hazards (e.g., earthquake and tsunami).

Defense in Depth (DiD)

The defense in depth is an engineering concept to protect people and environment from radiation risk, using multiple barriers with diverse characteristics.

Objective of each level in defense in depth

Levels of defense in depth	Objective	
Level 1	Prevention abnormal operation and failures	
Level 2	Control of abnormal operation and detection of failures	Up to level 3 design based on the design basis ground motion
Level 3	Control of accidents within the design basis	
Level 4	Control of severe plant conditions, including prevention of accident progression and mitigation of the consequences of severe accidents	Protection against DEC (Design Extension Condition) Probabilistic & deterministic risk assessment is used to analyse DEC
Level 5	Mitigation of radiological consequences of significant releases of radioactive materials	

Though, it is considered that each level of DiD must be independent, it is possible that functions for SSCs in each levels take damage simultaneously due to external events such as earthquake.

Therfore

Independence between each level of DiD cannot be approved in a strict sense. Diversity of SSCs is considered to be a key concept for feasibility of the defense in depth concept against earthquake.

Concept

Attenuation Relationship and Period-to-period correlation model

Ground motion is usually predicted using attenuation relationship. Attenuation relationship is statistical equation to predict acceleration response spectrum (Sa(T)). Itoi et al. (2015) proposed the attenuation relationship of spectral correlation for crustal earthquake as follow;

$$\log(Sa(T)) = a + bMw + cX - \log(X + d\cdot 10^{0.5Mw}) + e\cdot\{\log(Vs_{30})\} + f\cdot\log(Vs_{30}) + g\cdot\log(\max(\min(Z_{1500}, h), k)) + \varepsilon_{Inter} + \varepsilon_{Intra}$$

M_W : Moment magnitude
X : Fault shortest distance (km)
V_{S30} : The average S-wave velocity of the ground up to the surface 30m (m/s)
Z_{1500}: Depth of S-wave velocity is 1500(m/s) (m)
a~k : Regression coefficient
ε_{inter}, ε_{intra} : Inter-event and intra-event residuals

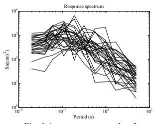

Fig. 1 Assessment example of acceleration response (the number of samples is 30)

A model for period-to-period correlation of intra and inter event residual ($\epsilon_{intra}, \epsilon_{inter}$) was also proposed.

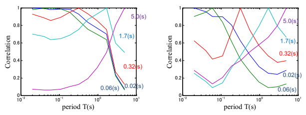

Fig.2 Correlation of ground motions. Left figure shows correlation of ε_{intra} and right figure shows correlation of ε_{inter}

T. Itoi, M. Murakami and N. Sekimura, "Statistical equations of response spectra of crustal earthquake for assessment of multiple facilities seismic risk" *Journal of JAEE*, Vol.15, No.6, pp 126-141, (2015)

Probabilistic Seismic Hazard Analysis

probabilistic seismic hazard analysis is to quantify the rate of exceeding various ground-motion levels at a site given all possible earthquakes. The following formula is used for seismic hazard assessment.

$$\nu(a) = \Sigma\Sigma\nu\cdot f(m_i)\cdot f(r_j)\cdot(f_{mi,rj}(a))$$

ν : Earthquake frequency in each of the earthquake epicenter area
$f(m_i)$: Frequency that the magnitude is m_i
$f(r_j)$: The probability that the distance from a target spot to the seismic center will be r_j
$f_{mi,rj}(a)$: The probability that the strength of the ground motion that takes into account the variation of the attenuation relationship is larger than a when magnitude is m_i and seismic center distance is r_j

Probabilistic Scenario Earthquake

Scenario Earthquake

Earthquake source

Assumption of one earthquake source
・Magnitude ・Location

Advantage

Easy to understand

Disadvantage

No relation to safety requirement of NPR

Probabilistic Seismic Hazard Assessment

Earthquake source

All the possible sources are considered

Advantage

The relationship between earthquake characteristics and the probability of occurrence

Disadvantage

Information such as magnitude and the seismic center distance of individual earthquakes is hidden

Probabilistic Scenario Earthquake

Probabilistic scenario earthquake is assessment method by assuming the highest contribution earthquake as a scenario earthquake. It makes it possible to objectively determine the scenario earthquakes corresponding to the specific risk level

Deaggregation

Hazard curve → Extraction of scenario earthquake with high contribution
Target probability level → Extraction of scenario earthquake with high contribution

H. Kameda, Y. Ishikawa, T. Okumura and M. Nakajima, "Probabilistic scenario earthquakes –definiton and engineering applications-", *Journal of JSCE*, Vol.577, pp. 75-87, (1997).

Proposed method

Hazard curve → Design point; Hazard curve → Scenario earthquake for SSCs in DiD level 4
Fragility curve for core damage → Design point → Scenario earthquake for SSCs in DiD level 4

The Conditional Mean Spectrum (CMS)

The CMS provides the expected response spectrum, conditioned on occurrence of a target spectral acceleration value at the period of interest.

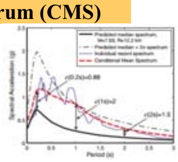
Fig. 3 Conditional mean values of spectral acceleration at each period

Distributed probability vector Z=(X',Y')

Mean vector $\mu = \begin{pmatrix}\mu_1\\ \mu_2\end{pmatrix}$ Variance matrix $\Sigma = \begin{pmatrix}\Sigma_{11} & \Sigma_{12}\\ \Sigma_{21} & \Sigma_{22}\end{pmatrix}$

When X is decided, Y gets the following functions;

$$Y|X = x \sim \phi(y; \mu_2 + \Sigma_{21}\Sigma_{11}^{-1}(x - \mu_1), \Sigma_{22} - \Sigma_{21}\Sigma_{11}^{-1}\Sigma_{12})$$

J.W.Baker, "Conditional mean spectrum: Tool for ground-motion selection", *J. Struct. Eng*, Vol.137, pp.322-331,(2011)

Example

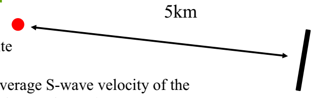

The average S-wave velocity of the ground up to the surface 30m(V_{S30}) : 700(m/s)

Depth of S-wave velocity is 1500 (m / s)(Z_{1500}) : 1000(m)

Fault
Magnitude : 6.6
Occurrence frequency : 1/50(/year)

Fig.4 Example of site and earthquake fault for calculate

The natural period of SSCs is usually very short (e.g., <0.1s). Sa(T=0.02s) is used for the index parameter for hazard and fragility. Setting the fragility curve as probability of failure is 10^{-3} in the design earthquake

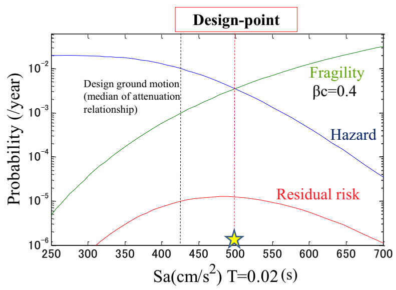

Fig.5 Hazard curve, fragility curve and residual risk calculated from example fault

Design point is most probable ground motion where accident occurs

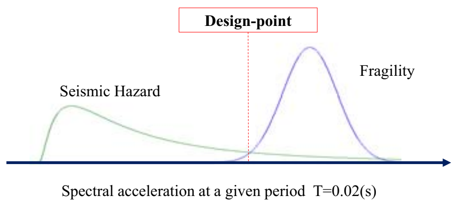

Fig.6 Relationship of hazard curve, fragility curve and design point

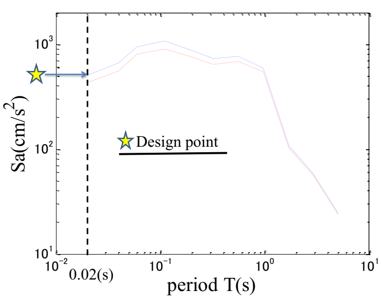

Fig.7 Assessment example of CMS

Table. 1 The difference of the design earthquake due to the periodic

	Period (s) 0.02	2.9
Scenario earthquake for level4	502.8 cm/s²	58.4 cm/s²
Design earthquake for up to level 3	426.7 cm/s²	56.6 cm/s²
Level 4 / Level 3	1.18	1.03

Ground motion of the design point is 1.18 times larger than the design earthquake ground motion, SSCs for Level 4 DiD with short natural period need to resist earthquake ground motion larger than the design basis.

SSCs with longer natural periods can function without changing design so much. (The strength of period 2,9(s) with the conditions has not been only 1.03 times)

Diversity is obtained by providing several different SSC of natural period

Conclusion and Future Work

Conclusion

- A method for estimation of earthquake scenarios for SSCs for Level 4 DiD was proposed
- Response spectra of the proposed earthquake scenario was calculated by combining the CMS and design point concept.
- Diversity of SSCs which can be obtained by changing the period is considered to be effective.

Future work

- A method for estimation of earthquake scenarios including distance as a parameter for SSCs in DiD level 5

Preliminary Study on Random Number Generation Method for Fragility Assessment

R. Tanaka(1), T. Itoi(2) , N. Sekimura(3)

(1) Master student, Graduate School of Engineering, The University of Tokyo, Tokyo, Japan, tanaka@safety.n.t.u-tokyo.ac.jp

(2) Associate Professor, Graduate School of Engineering, The University of Tokyo, Tokyo, Japan, itoi@n.t.u-tokyo.ac.jp

(3) Professor, Graduate School of Engineering, The University of Tokyo, Tokyo, Japan, sekimura@n.t.u-tokyo.ac.jp

Introduction

Objective

・For carrying out a seismic fragility analysis of SSCs (Structure, Systems and Components), so called "response factor method" is conventionally used. Fragility analysis using nonlinear dynamic response analysis is considered to more accurate because more realistic failure mode can be considered in dynamic response analysis. To obtain a fragility curve, a large number of dynamic response analyses needs to be conducted using Monte Carlo method.

・A large number of dynamic response analyses (i.e., a large number of random numbers) needs to be conducted to obtain a seismic fragility curve.

・ Because of limitation of performance of computer, it is desirable if it is possible to obtain an accurate result by few number of trials.

・ In this presentation, efficiency of two random number generation method (i.e., crude Monte Carlo sampling and Latin hypercube sampling) are compared by solving a simple example considering both aleatory and epistemic uncertainty.

Process of Seismic PRA [1]

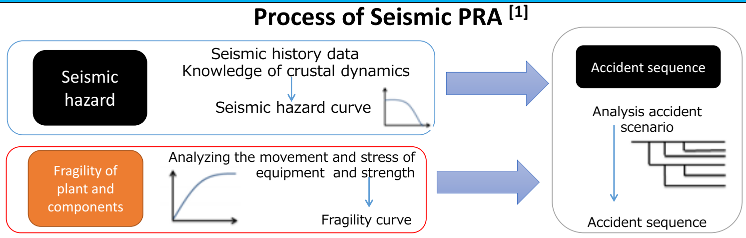

PRA (Probabilistic Risk Assessment)

Purpose

To know as many possible future adverse as possible

Prediction and prevention of unexpected accident

Analysis safety and make a plant safer

‣ The table below shows the list of accident-induced events.

Classification of accident induced event

Internal event	External event	
	Natural event	Human induced event
Random failure Internal fire Internal flood Turbine generated missile	Seismic Tsunami Volcano meteorite	Aircraft Transportation Terrorism

Fragility Assessment of Uncertainty

Seismic Fragility Assessment[2]

In seismic fragility analysis, failure probability is quantified using realistic response and realistic (obtained e.g., by dynamic response analysis) capacity of SSC.

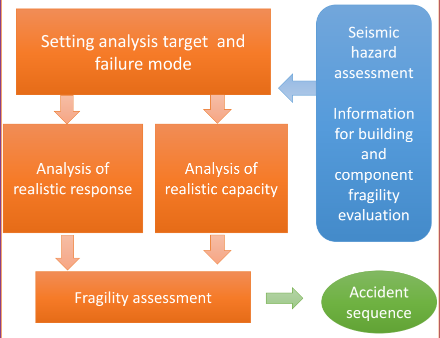

Two Types of Uncertainty [3]

Aleatory uncertainty

The aleatory uncertainty is associated with the randomness or inherent variability of nature, it is non-deterministic and therefore requires a random variable representation.

Epistemic uncertainty

The epistemic uncertainty is due to our inability to correctly predict or estimate reality (which may be deterministic) and thus involves a range of possible errors.

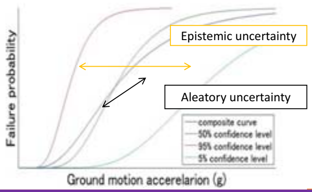

Uncertainty in fragility assessment

・Both aleatory and epistemic uncertainties are considered in estimation of realistic response or capacity.

・For example, in realistic response analysis, uncertainty in parameters (e.g., ground motion time history, stiffness and damping of structures) are considered. In a fragility analysis using dynamic response analysis , input seismic motion or seismic response analysis model are randomly generated considering both aleatory or epistemic uncertainties.

Image of Realistic response

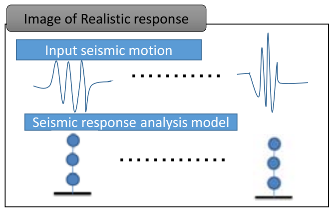

Random Number Generation Methods

Random Number Generation Method

・Two methods are compared from the viewpoint of efficiency.

Monte Carlo simulation

・The method to calculate repeatedly mathematical or empirical operator that has variable which includes uncertainness followed random variable or the probability distribution which was appointed

Latin hypercube sampling [4]

・In Latin hypercube sampling (LHS), accumulation probability of each parameter is divided into n and sampled by once from each section at random.

・Fig.1. [5] shows the example of LHS. Dot presents parameter and grid presents separation point. There are one parameter in adjacent separation point.

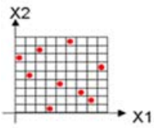

Fig.1. Example of LHS [5]

Example Problem to Compare LHS and MS [6]

・To compare how much difference is in Latin hypercube sampling and Monte Carlo simulation, I solved simple example. Find a solution of Failure probability P_F with Aleatory uncertainty; P_F=P(R-S<0). And R and S are expressed in each probability distribution. More, there are epistemic uncertainty which is expressed in probability distribution in μ_R and μ_S and find standard deviation of mean of failure probability on each trial.

example

Failure probability with Aleatory uncertainty; P_F=P(R-S<0)

R=N(40*Re,15), S=LN(25*Re,0.35)

Where, Re and Se are represent epistemic uncertainty in mean value of R and S, respectively, as follows:

Re=N(1.0,0.10), Se=N(1.0,0.15)

and using LHS or MC, find standard deviation of mean and of failure probability on each trial.

More, find a solution of P_F with no epistemic uncertainty (R=N(40, 15), S=LN(25, 0.35))

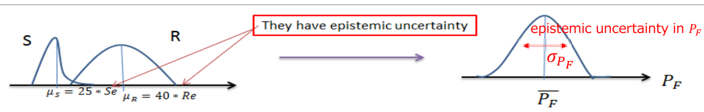

Results and Conclusion

Results of the Example

standard deviation of $\overline{P_F}$ with uncertainty

Number of trials	50	200	500
MC	0.0148	0.0058	0.0044
LHS	0.0048	0.0012	0.0007

・In same number of trial, accuracy of LHS is about 3〜6 times higher.

$\sigma_{\overline{P_F}}$ Statistical error in estimated $\overline{P_F}$

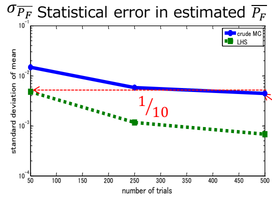

Fig.3. accuracy comparison of LHS and MC of P_F with uncertainty

Fig. 3. shows that LHS needs one tenth number of trials to get same statistical error in estimated $\overline{P_F}$ and compared to MC and the gap between the two is increased.

This red line presents $\sigma_{\overline{P_F}}$ of MC when x is 500.

$\sigma_{\overline{P_F}}$ Statistical error in estimated $\overline{P_F}$

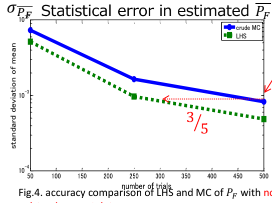

Fig.4. accuracy comparison of LHS and MC of P_F with no epistemic uncertainty

Fig. 4. shows that LHS needs three fifth number of trials to get same statistical error in estimated P_F compared to MS. However the gap between them is smaller than that with epistemic uncertainty.

Summary and Future Work

・Solving the example, how much difference is in Latin hypercube sampling and Monte Carlo simulation is compared. The result of example shows that using Latin hypercube sampling, same statistical error can be obtained by few number of trials than Monte Carlo simulation. More, those differences spread so that amount of calculation increases.

・In my future work, a method for seismic fragility analysis using LHS and nonlinear dynamic analysis will be proposed to discuss its advantage.

references

[1] Stan Kaplan, Harold F. Perla, Dennis C. Bley, "A Methodology for Seismic Risk Analysis of Nuclear Power Plants", Risk Analysis, vol.3. No.3(1983)

[2] Atomic Energy Society of Japan 'A standard for Procedure of Seismic Probabilistic Risk Assessment for nuclear power plants : 2007'

[3] A. H.-S. ANG,D. DE LEON,' Modeling and analysis of uncertainties for risk-informed decisions in infrastructures engineering' ,Structure and Infrastructure Engineering, Vol. 1, No. 1,pp.19 – 31(2005)

[4] Takeshi Goda, Kozo Sato, 'Global optimization of well placement for geological storage of CO2 using iterative Latin hypercube samplings' Journal of the Japanese Association for Petroleum Technology, Vol.76,No.3,pp.233-243(2011)

[5] http://www.quint.co.jp/jp/pro/amd/amd_fnc-kmd.htm

[6] Alfredo H-S. Ang, Wilson H. Tang, 'Concepts in Engineering: Emphasis on Applications to Civil and Environmental Engineering' , (2006)

The Analysis of Sand Movement and Erosion Monitoring along the Northern Coasts of Vietnam

Ryota HIGASHI, Y. Tajima, K. GUNASEKARA The University of Tokyo

Resilience of Coastal Zone

Coastal erosion has been dominantly observed within the past 10~30 years around the Red River mouth and the erosion appears to be expanded toward the Ma River within the past 10 years.

Questions are:

- ✓ What are the primary factors which cause coastal erosion around the Ma River?
- ✓ Does the Red River have influence on the erosion around the Ma River?

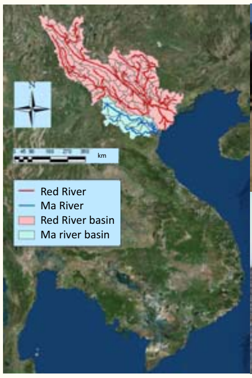

Methodology

Sediment

Grain size

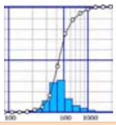

Color

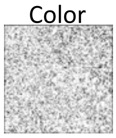

Thermo Luminescence

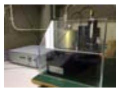

Alongshore Distributions of Sediment Characteristics

➕

Shoreline Changes in Space and Time

⬇

Apply 1-line model

⬇

Understand the sediment transport characteristics

Satellite

Shoreline extraction

Quantitative analysis of shoreline change

Characteristics of River Discharge

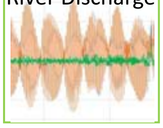

Sediment Analysis

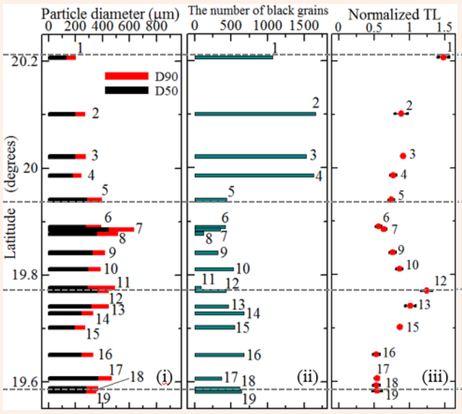

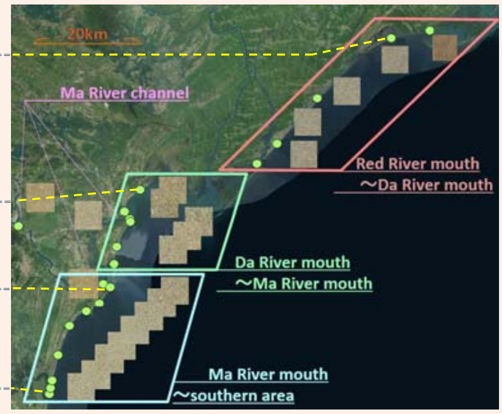

Grain characteristics

(i) D50 and D90: The Ma River may have more dominant influence on the sediment budget along the coast around the Ma River mouth.

(ii) The number of black grains: Clear gap between the coast around the Red River and the Mar River also supports our hypothesis that the Red River has little influence on sediment budget along the coast around the Ma River mouth

(iii) intensity of TL: Little sand supply to southern area from the Ma river

Satellite Analysis

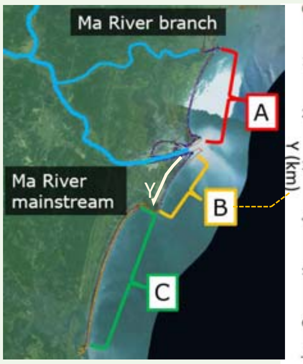

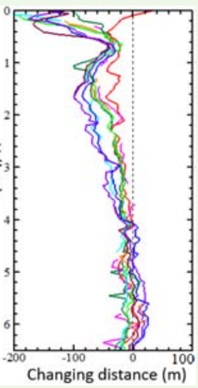

Around Ma River mouth

(i) A&C: The entire shoreline was deteriorated from 2000 to 2005 but shoreline have been relatively **stable** in the past 10 years.

(ii) B: Severe erosion around the river mouth while the southern part has been stable or has shown slight accumulation in the past 10 years.

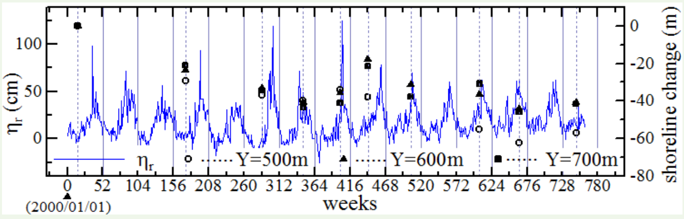

Comparing variation of shorelines and water level

There are a correlation between River water level and precipitation / water level and amount of sediments

➡ **Seasonal sediments variation don't influence shorelines.**

1-line Model Prediction

■ Purpose

Estimate shoreline change and alongshore budget of sediment transport

Calibration
- ✓ slope
- ✓ wave direction
- ✓ amounts of sediments

et. all.

calibration

Calculate
- ✓ 2D wave
- ✓ amounts of coastal drift sand
- ✓ shoreline change

Satellites Analysis

Analysis of sediment grains
→no influence from the Red River

continuous equation of sediments

$$\frac{\partial x_s}{\partial t} + \frac{1}{D_s}\left(\frac{\partial Q}{\partial y} - q\right) = 0$$

Thermo Luminescence

estimate supply sediments
→Little sediment supply from the river mouth

x_s : shoreline location, D_s : Critical water depth of sand movement,
Q : Total flux of littoral drift, y : *alongshore location*, q : sediment supply from the river

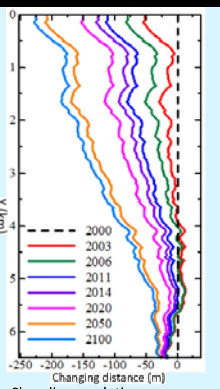

Shoreline evolution predicted by 1-line model

Conclusion

1. Red River so far has little influence on the coastal erosion around the Ma River.
2. Severe erosion was dominantly observed around the Ma River mouth while other areas were relatively stable.
3. Shoreline model reasonably represents the observed shoreline change in the southern part of the Ma River mouth.
4. Sediment supply from the Ma River may have been significantly reduced in the past 20 years but the shoreline may reach to static equilibrium conditions in the next 100 years or so.

A Study on Nearshore Topography Estimation by Using UAV

Yoshinao MATSUBA, Shinji SATO, The University of Tokyo

RISKS FOR COASTAL URBAN SYSTEM

Construction of artificial structures, such as ports, jetties, caused terrible coastal erosion.

- The coastal urban system will receive huge damage by typhoon storms.
- Various engineering methods to protect nearshore area from erosion are tested these days, and we need to examine their effectiveness correctly.

⬇

We need to monitor changes of nearshore topography frequently. However, it takes a lot of costs and time to monitor them frequently. In this study, a new monitoring technique is developed for nearshore topography.

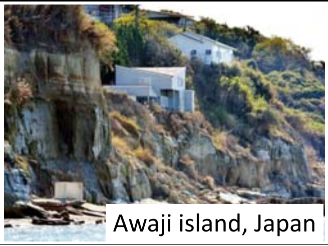

Awaji island, Japan

NEW MONITORING SYSTEM

Sea area

Shooting video of sea surface at a high altitude (using UAV)

⬇

Detecting wave-crest lines (Used wavelet transformation)

⬇

Calculating wave-celerity and wave-period

⬇

Estimating water depth by dispersion relation

$$C = \frac{gT}{2\pi} \tanh \frac{2\pi h}{CT}$$

⬇

Estimating the topography

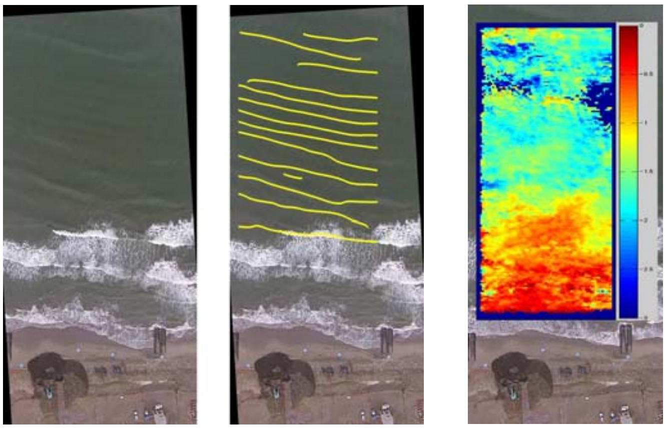

Land area

Using SfM model

SfM(Structure from Motion):the process of estimating 3-dimensional structures from 2-dimensional image sequences which may be coupled with local motion signals.

By using pictures taken by UAV, estimating the topography of land area with the method.

UAV

Picture taken by UAV

Result of SfM

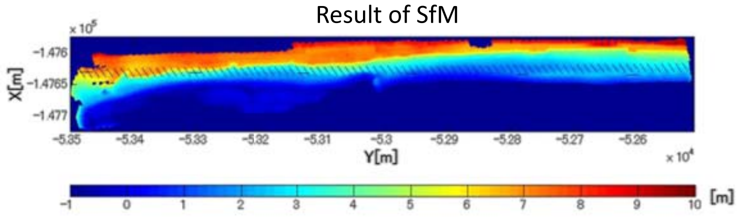

APPLY THE NEW SYSTEM

Fukude port and Asaba coast

- Because of the construction of Fukude port, deposition occurred on the western side of the port and terrible erosion occurred at Asaba coast, on eastern side of the port.
- To solve these problems, sand-bypassing system has been introduced in October, 2015(First time in Japan).
- High resolution/high frequency monitoring is expected to capture dynamic topography changes.
- We conducted monitoring in August, 2015 and January, 2016 using the new system.

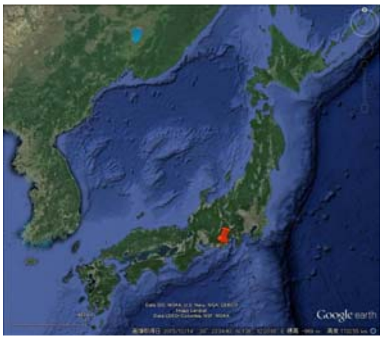

↑Sand-bypassing system

Outlet→

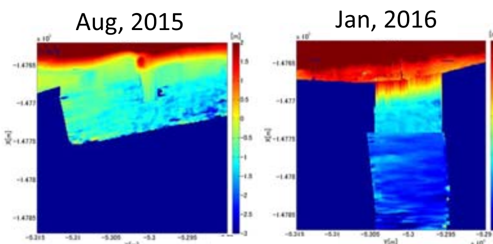

Increment

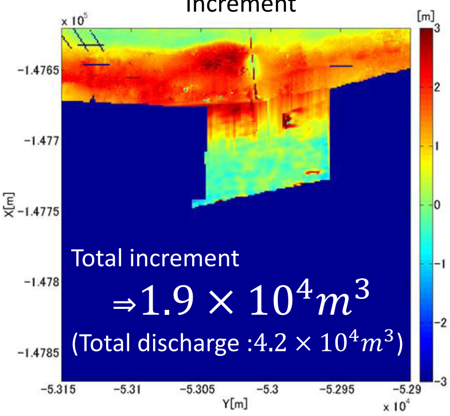

Two Phase Flow Effect on Single Turbine Blade

Erdal Özdemir, Nejdet Erkan, Byeongman Jo, Koji Okamoto

The University of Tokyo

1. Introduction

- In BWRs RCIC system provides makeup water to RPV for core cooling to compensate for water being boiled away by the decay heat.
- As measurement systems failed no one has clear explanation about RCIC behavior after station blackout.
- 3 days operation of RCIC system delays core melt in Fukushima Unit-2 and some part of the melt suspected to be remained in the core.
- The mixture of steam and water may have carried energy equivalent to that of the decay heat to the RCIC turbine resulting in power degradation.

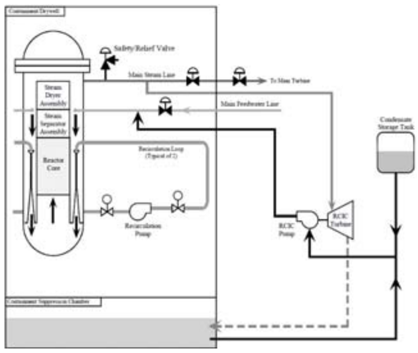

USNRC Technical Training Center. Boiling Water Reactor GE BWR/6 Technology Technology Manual. Chapter 2.7 Reactor Core Isolation System.

2. Objectives

- Critical components behavior under beyond design basis conditions
- Effect of two-phase flow on turbine efficiency
- Investigating the effect of two-phase flow on turbine efficiency with single blade experiments

3. Single Blade Experiment

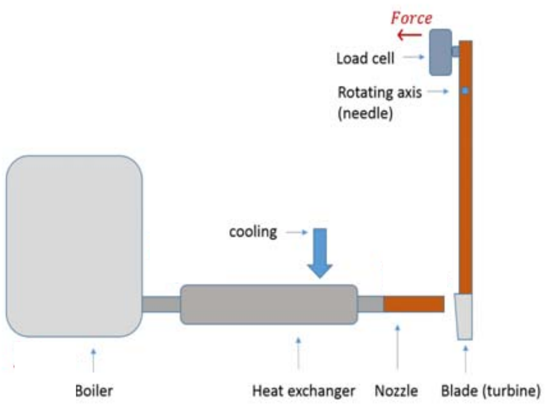

4.Critical Flow

Energy Balance

$$W_{cooling} = W_{condensation}$$

$$x = \frac{\dot{m}_c C_p \left(T_{c_{out}} - T_{c_{in}}\right)}{\dot{m} L_v}$$

Single Phase Critical Flow

$$0 = h_o - \left(h_b + \frac{v_b^2}{2}\right)$$

$$G_b = \rho_o \sqrt{2 c_p T_o \left[\left(\frac{p_b}{p_o}\right)^{\frac{2}{\gamma}} - \left(\frac{p_b}{p_o}\right)^{\frac{\gamma+1}{\gamma}}\right]}$$

Two Phase Critical Flow

$$0 = h_o - \left[x h_g + (1-x) h_f + x\frac{v_g^2}{2} + (1-x)\frac{v_f^2}{2}\right]$$

$$x = \frac{s_o - s_f}{s_g - s_f}$$

$$\{\alpha\} = \frac{1}{1 + \left[\frac{(1-x)}{x}\right]\left(\frac{\rho_v}{\rho_l}\right) S}$$

$$\rho^{''} = \left\{\left[\frac{x}{\rho_g} + \frac{(1-x) S}{\rho_f}\right]^2 \left[x + \frac{1-x}{S^2}\right]\right\}^{-0.5}$$

$$G = \rho^{''} \sqrt{2\left[h_o - x h_g - (1-x) h_f\right]}$$

5. Experiment Results

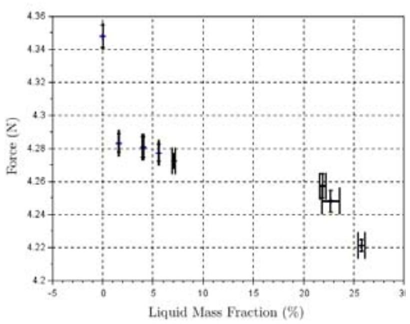

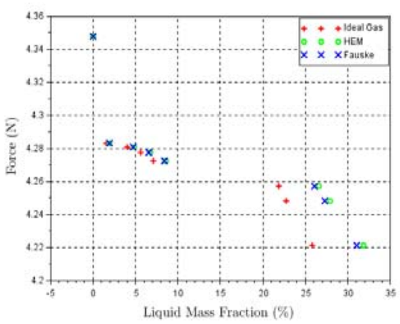

6. Conclusion

- Force is decreasing with increased liquid mass fraction in single blade experiment.
- Analysis with single phase gas assumption well agree with commonly used two phase flow models.
- More detailed analysis with full scale tests may reveal better results about power degradation of RCIC turbine.

Simulation of three-dimensional vibrational characteristics of mountains

３次元形状を考慮した山体の振動特性に関する数値シミュレーション

Shogo Shimizu, Hiroaki Yamanaka, Koichiro Saguchi, Kaoru Kojima

(Dept of Environmental Science and Technology, Tokyo Institute of Technology)

Abstract

Natural frequencies of soil and buildings are controlled by their physical property and regarded as one of fundamental characteristics in their vibration. We usually can identify a Natural frequency from a largest peak of spectrum of vibration data. However, identification of a Natural period is sometimes difficult for a building with a three-dimensionally complex shape. Kojima (2013) focused on the Natural frequency of Mt. Fuji, from an analysis based on microtremor observation data and interpreted the vibration characteristics from FEM analysis. However, many mountains existing in Japan have mountain-range shape such as Tateyama Mountain range and Yatsugatake Mountain.

In this research, I simulated vibration of various mountains with different shapes using finite element method (FEM). I firstly conducted FEM analysis using an elastic mountain models with simple three-dimensional shapes considering mountain range. Natural frequency for the mountain range model differs from single peak mountain model indicating huge effects of three-dimensional shapes. I next conducted FEM analysis for real shapes model of Mt. Yatsugatake based on the digital elevation data. The results show that Natural frequencies in long-side and short-side directions are different from each other. And vibration modes are also different between in higher and lower locations.

■Numerical simulation of simple models

①Making simple models

Model is totally created 20 pcs. I Changed the bottom surface ratio(1:1~1:5), and height(1.0km~2.5km) increase by 0.5km. 1:1 model is assumed by single-peak mountains. 1:2~1:5 models are assumed by mountain-range.

I use homogeneous Physical properties to analyze(It is determined by one Research Commission in Japan in 2001 for Tokai area's disaster prevention) shown as Table1.

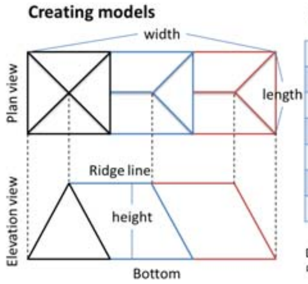

Fig.1 Making Models

Physical properties (Homogeneous)

Density ρ [kg/m³]	2400
S wave V_S[m/s]	2500
P wave V_P[m/s]	4600
V_P/V_S ratio	1.84
Young's modulus E[Pa]	3.87×10^{10}
Poisson's ratio ν	0.29
Mesh size[m]	500

Determined by Research Commission in Japan.
中央防災議会 東海地震に関する専門調査会(2001)

Table.1 Physical properties

②Analysis result of simple models

I focused on Primary mode because it is most dominant mode in the model. I found both of short and long side's Primary mode was First mode in all models.

Fig.2 is the graph that the analysis result of Natural frequency by each models. I fixed height 1.5km and changed the ratio of short side length and long side length 1:1~1:5. Fig.3 is also the graph of Natural frequency that I fixed bottom surface ratio 1:3 and changed height 1.0~2.5km.

1:1 model that assumed single-peak mountains models have same Natural frequency and it means this shape model has no directional dependence. However, mountain-range models have different Natural frequency and directional dependence. About the relation between model height and Natural frequency, the higher models are, the smaller Natural frequency is.

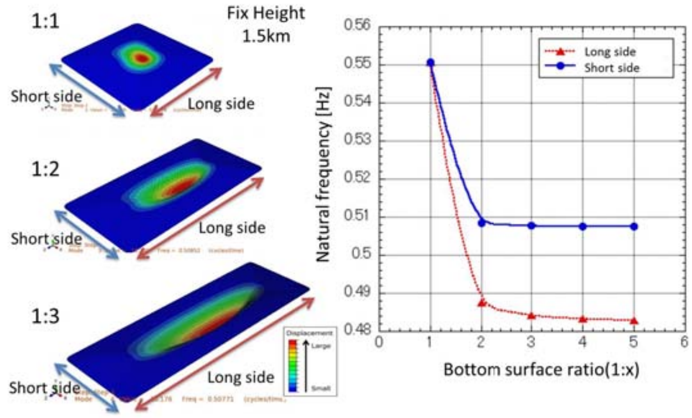

Fig.2 Relation of Bottom surface ratio and Natural frequency

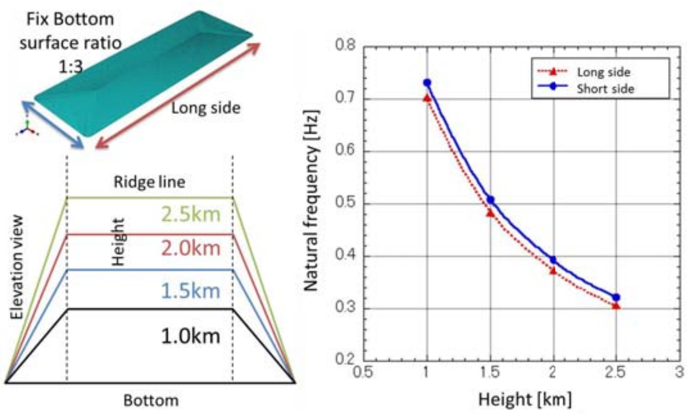

Fig.3 Relation of Height and Natural frequency

■Numerical Simulation of Mt.Yatsugatake model

① Making a real model

I create Yatsugatake model over the altitude 1200m based on elevation data. The element shape is tetrahedral element, mesh size is 500m split(Fig.4). Bottom left figure is cross-sectional view drawn by red line along the ridge on the topographic map, and the characters show the main places in Mt.Yatsugatake. Physical properties are same as Table.1.

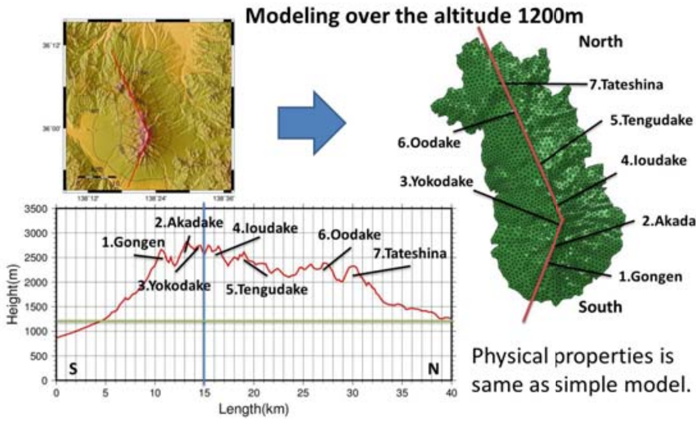

Fig.4 Mt.Yatsugatake Model

②Analysis result of Mt.Yatsugatake model

Dominant Vibrational mode come out multiple, because it is a complex model. The first mode has one peak of vibration, the secondary mode has two peaks, and Third mode has three peaks on each direction. And the results of the analysis, the most contributing Vibrational mode to this model, is the first mode framed by red line, and then, second contributing mode is Third mode framed by blue line(Fig.5). As the analysis, secondary mode does not substantially contribute. In the first mode, Akadake, Yokodake, Ioudake is vibrating well. In the Third mode, Gongendake and Tengudake is vibrating well.

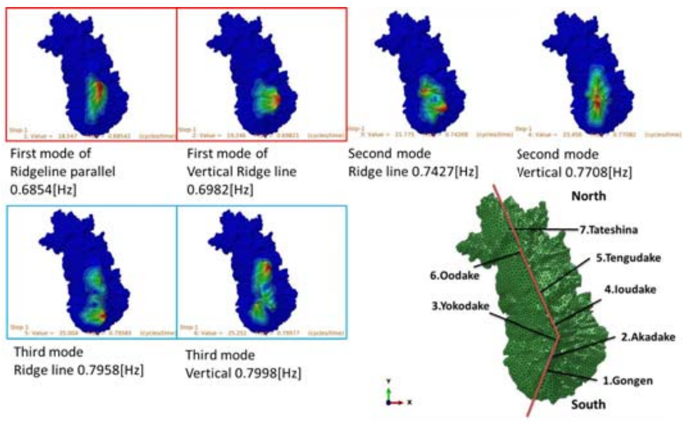

Fig.5 Vibration mode of Mt.Yatsugatake

■Conclusion

This research suggests that each mountains have each dominant Vibrational modes. Compare to single-peak model and mountain-range model, the results show that Natural frequencies in long-side and short-side directions are different from each other. And Vibration modes are also different between in higher and lower locations.

In Mt.Yatsugatake model, in higher part has greater vibration and the Vibrational mode is different by place in Mt.Yatsugatake. This clearly indicated that sensor direction and installation site must be carefully oriented in a field observation of vibration in Mt. Yatsugatake.

Future tasks are planning of observation in considering of the conclusion, and do the actual measurement in Mt.Yatsugatake. And modeling from observed data, considering estimated physical properties and internal structure.

Analytical Hysteresis Response of RC Shear Walls

Chanipa Netrattana
Professor Susumu Kono

Introduction

In 2010 Chile Off Maule Earthquake (AIJ 2010), a great number of RC walls damaged by flexural failures. In order to understand the characteristic of structural walls under earthquake, four 40% scale cantilever RC walls, two type configurations were tested (Kono et al. 2013).

In addition, the fiber analytical models were used to predict the structural response and verified with experimental results. Base on validated modeling scheme, more structural walls with various condition will be further studied in the future.

Objective

The objective of this study is to **predict the hysteretic curve as lateral force-drift angle relations by using simple fiber model** for studying seismic behavior of RC walls (NC40, NC80, BC40 and BC80).

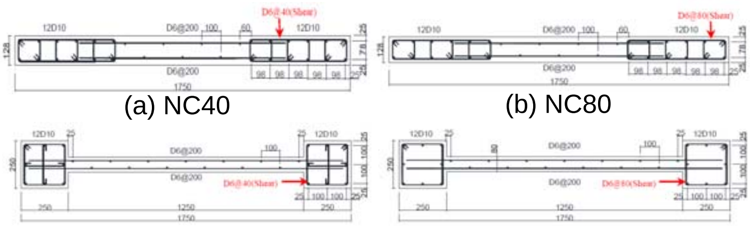

(a) NC40 (b) NC80

(c) BC40 (d) BC80

Plan view of specimens

Methodology

In fiber elements model, unconfined concrete elements are shown as yellow elements, while confined concrete elements are shown as blue elements. Each reinforcement steels are modeled by one element in fiber model.
In material model, confined concrete for cyclic loading is based on **Yassin (1994).** Reinforcement steel for cyclic loading complies with **bilinear rule**.

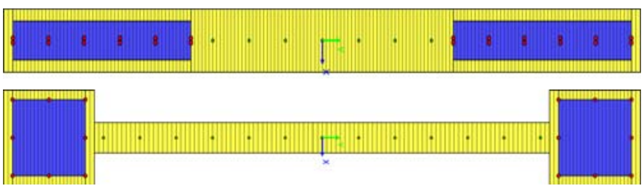

Elements in fiber model

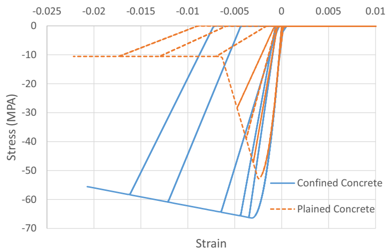

Stress-strain of concrete elements by Yassin (1994)

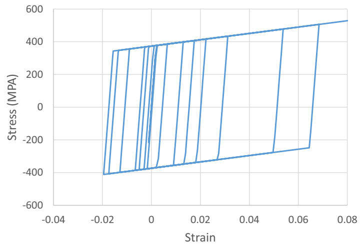

Stress-strain of steel elements by bilinear rule

Results and Discussions

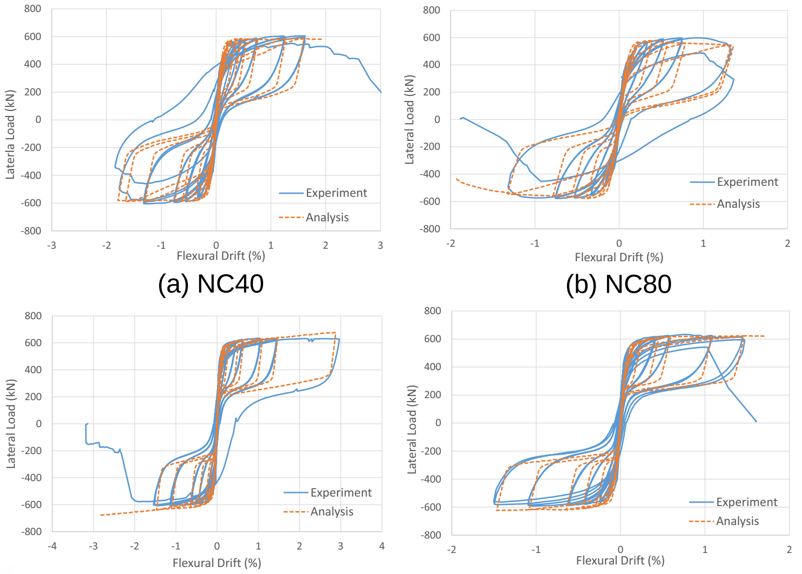

(a) NC40 (b) NC80

(c) BC40 (d) BC80

The results show that the model is able to predict the whole hysteresis responses of specimens correctly. The analytical behaviors such as stiffness, peak lateral load, ultimate flexural drift are good consistent with experimental result. However, the model can not simulate all behavior in each step perfectly. The model tends to slightly overestimate the stiffness of unloading curve. The cause might be too steep slope of stress-strain relationship of unloading path in concrete and steel model.

Conclusions

The fiber model are conducted to predict the hysteresis curve of four RC walls by using Yassin (1994) model and bilinear for concrete and reinforcement steel. The results show that the model is capable of analyzing overall nonlinear behavior of the RC walls with good accuracy. Although, analytical unloading path conflicts with experimental results.

Reference

Architectural Institute of Japan (2012). Reconnaissance Report on The 2010 Chile Off Maule Earthquake, pp. 313.
Kono et al. (2013), "Effect of Boundary Area Confinement on the Ultimate Flexural Drift Capacity of Cantiliver Structural Walls." *Proceeding of the 6th Civil Engineering in Asia Region*, Jakata, Indonesia.
Yassin, M. H. M. (1994). Nonlinear analysis of prestressed concrete structures under monotonic and cyclic loads. PhD Thesis. University of California, Berkeley, California.

1st Joint Workshop Japan-Turkey Cooperative Program on Resilience Engineering for Energy and Urban Systems

CYCLIC LOADING TESTS OF SUB-STANDARD RC FRAMES RETROFITTED WITH BUCKLING RESTRAINED BRACES AND ELASTIC STEEL FRAMES

Kazuhiro Fujishita (Tokyo Institute of Technology), Ahmet BAL, Fatih SUTCU, Ryota MATSUI, Masao TERASHIMA, Oguz C. CELIK and Toru TAKEUCHI

1. Introduction

Response control retrofit of existing RC buildings with buckling restrained braces (BRBs) assures immediate occupancy performance level after severe seismic events. This method is widely used in Japan and may improve the sub-standard buildings in overseas countries with high building importance factors e.g. school buildings in Turkey. Implementation of BRBs and elastically designed closed-steel frames in seismically deficient such RC frames would provide a much better damage distribution and mitigate the possible residual displacement after an earthquake. This research describes near full-scale displacement-controlled cyclic testing of five specimens to meet the performance requirements given by the relevant codes in Japan. Special emphasis has been placed on the composite interaction between the RC frame and added elastic frame. Experimental results including hysteretic curves, dissipated energies, crack patterns on the RC elements, and strain histories are promising for the response control retrofit of sub-standard RC buildings located in seismically vulnerable areas.

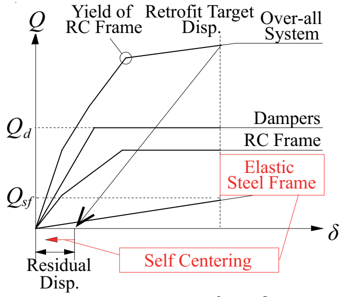

Figure.1 Concept of retrofit

Photo.1 A typical school building in turkey

2. Test Specimens

R model : RC bare frame

RS model : RC bare frame + Steel frame

RSB model : RC bare frame + Steel frame + BRB (attached inside frame)

RSBe model : RC bare frame + Steel frame + BRB (attached outside frame)

RSBF model : RC bare frame + Steel frame + BRB (attached inside frame) + FRP

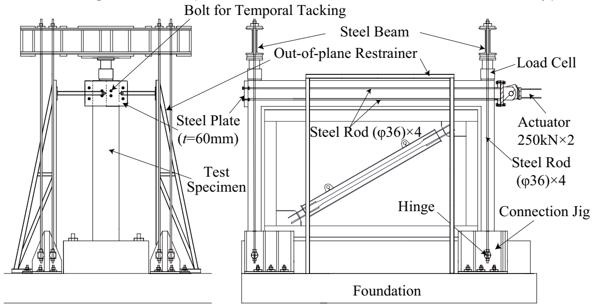

Figure.2 Setup of cyclic loading test

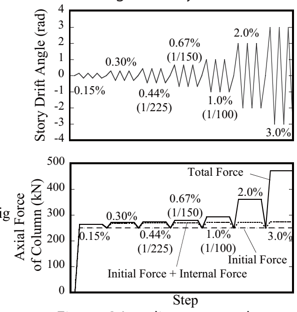

Figure.3 Loading protocol

3. Test Results

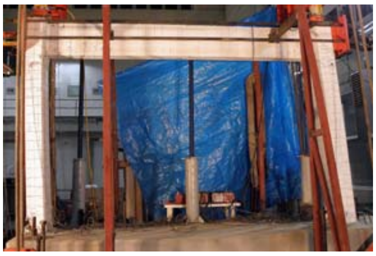

Photo.2 R model (after 4% 3cycle loading)

Photo.3 Bending collapse of RC column on R model

Photo.4 RS model (after 3% 9cycle loading)

Photo.5 RSB model (after 0.67% 9cycle loading)

Photo.6 RSBe model (after 0.67% 9cycle loading)

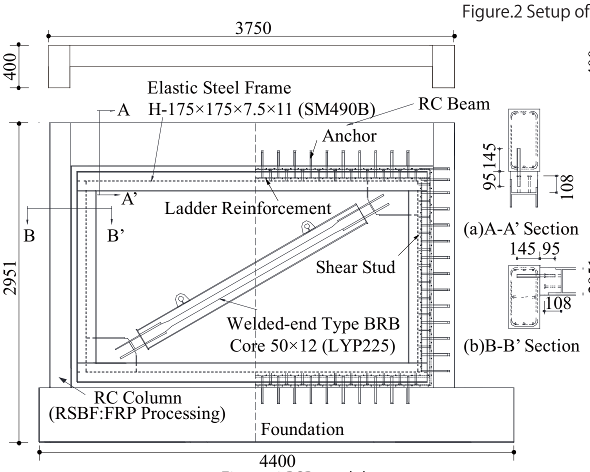

Figure.4 RSB model

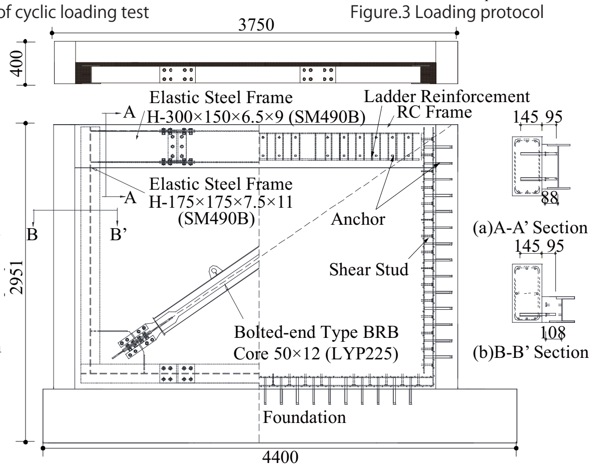

Figure.5 RSBe model

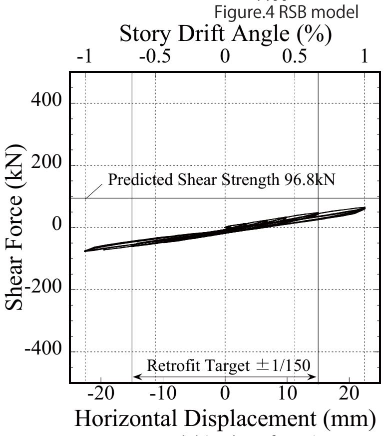

Figure.6 R model (RC bare frame)

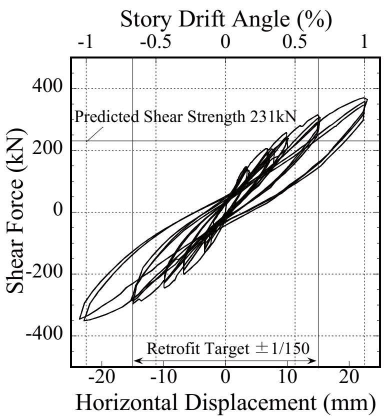

Figure.7 RS model (RC frame + Steel frame)

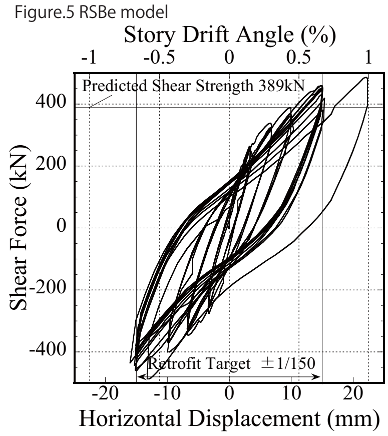

Figure.8 RSB model (RC frame + Steel frame + BRB)

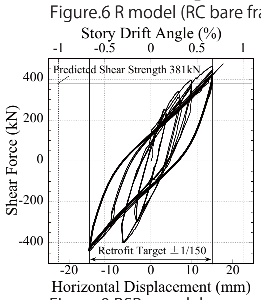

Figure.9 RSBe model

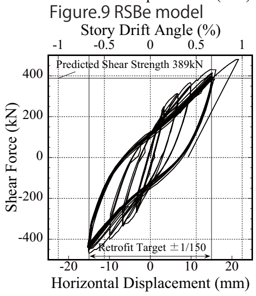

Figure.10 RSBF model

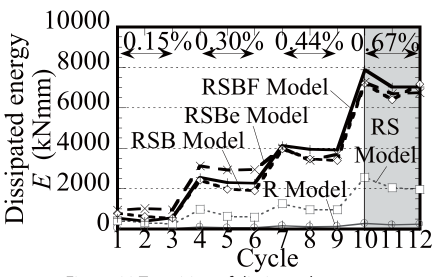

Figure.11 Transition of dissipated energy

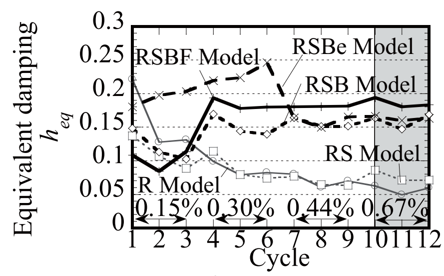

Figure.12 Transition of equivalent damping ratio

4. Conclusions

1) Retrofit specimens being arranged Buckling Restrained Brace and steel frame inside and outside RC frame dissipated sufficient earthquake energy on retrofit target story drift angle of seismic retrofit 0.67% and the effectiveness of proposed construction method for response control retrofit was confirmed. On the loading until retrofit target story drift angle, steel frame kept elastic and the maximum cracking width of RC frame was under 1 mm which satisfies the immediate occupancy of buildings. Connection collapse like panting shear was not observed on retrofit specimens.

2) On RSBF model introduced Fiber Reinforced Plastic to RC columns, the maximum strain of rebar on RC frame was smaller than other specimens and the structural damage was decreased. There are no significant strain and crack on the surface of FRP during loading on 0.67%.

Evaluation of Rayleigh-wave group velocities using seismic interferometry in the vicinity of Tachikawa fault zone, Japan

Hirokazu Ishige[1], Kosuke Chimoto[1], Koichiro Saguchi[1], Hiroaki Yamanaka[1]
Shinichi Sakai[2], Eiji Kurashimo[2], Naoshi Hirata[2]
[1] Interdisciplinary Graduate School of Science and Engineering, Tokyo Institute of Technology,
[2] Earthquake Research Institute the University of Tokyo

Abstract

Recently, it is emphasized that possibility of epicentral earthquake in Tokyo has become higher. For the purpose of improving present prediction of strong ground motion, I evaluated the surface-wave group velocities in the vicinity of Tachikawa fault zone which has around 30km length in Kanto basin, Japan, using seismic interferometry for continuous earthquake data. And finally compared the tomography maps of group velocities observed in this study with those calculated from existing subsurface structural model.

①Analysis Method

Seismic interferometry is a signal processing method calculating cross-correlation of ground motion between different two points that composes Green's function at one measurement point whose imaginary seismic center is another point. This enables to get signals from long-term continuous microtremors data which is considered as noise in usual seismic analysis (ex. Shapiro and Campillo,2006). Using this method, I conducted research based on the flow as shown in fig.1

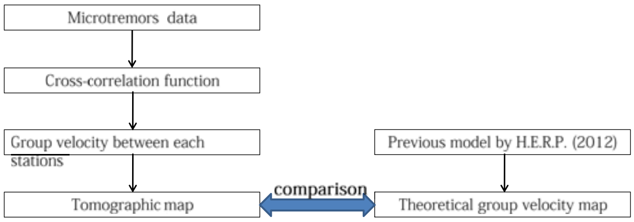

fig.1 Flow of this study

②Observed Data

The data I analyzed are microtremor portion of continuous seismic data from March 10th to 31th 2013, out of those observed by Earthquake Research Institute of The University of Tokyo. In order to reveal differences in characteristics of east and west side of the vicinity of Tachikawa fault zone, 30 measurement points were set temporarily, including two survey lines which roughly cross the fault line orthogonally(fig.2). However, only 28 points data were available in analysis because we failed to get data at the point No.4 and No.30.

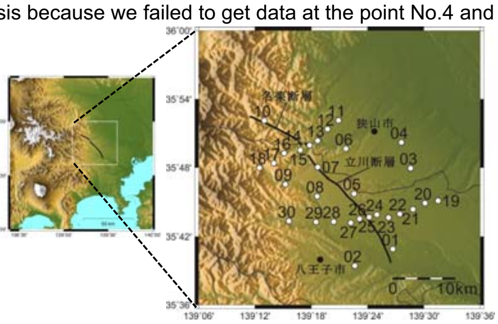

fig.2 30 measurement points in the vicinity of Tachikawa Fault Zone

③Cross-correlation Function

Data processing way following *Chimoto and Yamanaka(2012),* cross-correlation functions of vertical component were calculated from stacked microtremors data 378 combinations of pair of measurement points. Fig.3 shows some groups of cross-correlation function filtered in 2-4sec period which have distinguishing differences in velocity of wave propagation. Referring this results, northern and western part of southern survey line have faster propagation velocity than that of eastern part of southern line.

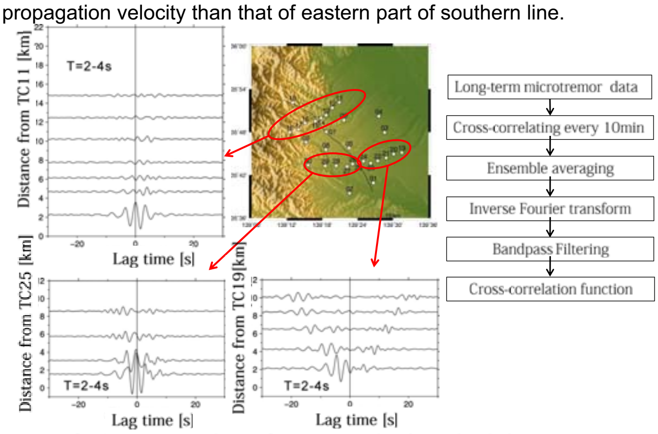

fig.3 cross-correlation functions in the three divided area

④Estimation of Group Velocities

Next I conducted multiple filter analysis(Dziewonski et al.,1969) in cross-correlation function to obtain dispersion curve of Rayleigh-wave group velocities(fig.4). These figures express bigger amplitude of cross-correlation function in darker color. You can read that clear signals appear in southern area, for example, the pair of 19-20(in southeastern area) has 0.5km/s velocity at the period of 3-4sec or less.

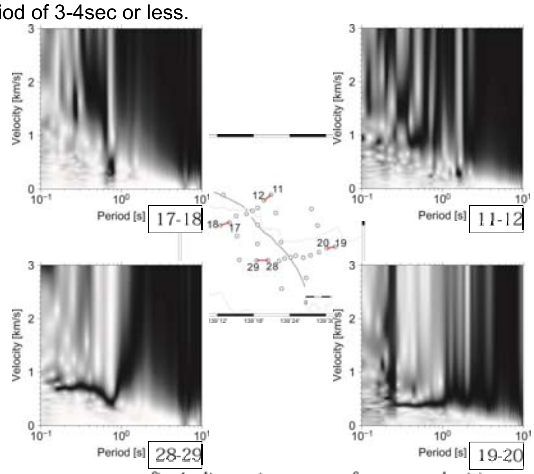

fig.4 dispersion curve of group velocities

⑤Tomography Analysis

Using the data extracted from estimated group velocities on the conditions that SN ratio(max. amplitude divided by noise RMS)exceeds 50, I carried out tomography analysis based on simultaneous iteration method(Clayton Comer, 1983). I finally compared the group velocities observed from seismic interferometry with those calculated from existing subsurface structural model "Prediction Map for Long-period Earthquake Motion"(the Headquarters for Earthquake Research Promotion,2012). The results show that the high group velocity area found in the southwest side become wider at shorter period band than those in the anamnestic model.

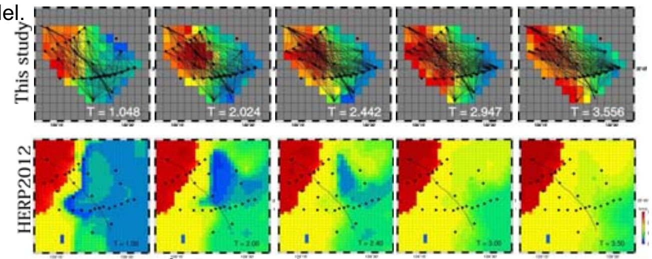

fig.5 tomography maps in comparison to those obtained from the Headquarters for Earthquake Research Promotion

⑥Conclusion

Rayleigh-wave group velocities were calculated using seismic interferometry for microtremor data of continuous seismic observation in the vicinity of the Tachikawa fault zone. As a result, distinguishing signals appeared at around 1-5sec period band, and tomography analysis revealed faster group velocities are measured in the western area of the fault zone than those in the eastern area. It can be said that effects of existence of the fault is remarkable because compared with existing subsurface structural model, maps obtained in this study show that the boundary between higher velocity area and lower area lies along the fault line. Only vertical component of ground motion was handled in this study because our target was Rayleigh-wave, but we will conduct analysis for horizontal, radial, and transverse component in future activities so as to improve constructing subsurface structural model in the vicinity of the Tachikawa fault zone.

Seismic Shear Force Amplification in Post-Tensioned Hybrid Precast Walls

H. A. D. Samith Buddika and Anil C. Wijeyewickrema
Department of Civil Engineering, Tokyo Institute of Technology, Tokyo, Japan

Abstract: In recent years, post-tensioned hybrid precast wall systems have been developed as an alternative for monolithic cast-in-place reinforced concrete (RC) shear walls to use as lateral-force resisting system in buildings located in seismic prone regions. These hybrid precast walls incorporate unbonded post-tensioned (PT) tendons that extend from the roof-level to the foundation-level and energy-dissipation (ED) dampers installed at the base of the wall. Self-centering response of hybrid precast walls is achieved by restoring forces provided by gravity loading and PT force. In post-tensioned hybrid precast walls, damage at the base of wall is eliminated by allowing gap opening/closing at the wall-foundation interface (rocking behavior), while at the same time dissipating sufficient amount of energy using damper devices. However, seismic shear amplification in post-tensioned hybrid precast walls is not well understood. Design guidelines and requirements for walls satisfying ACI ITG-5.1-07, that is ACI ITG-5.2-09 simply refer to Eberhard and Sozen (1993) for the seismic shear design.

The Problem

Shear slip failure at the wall foundation interface

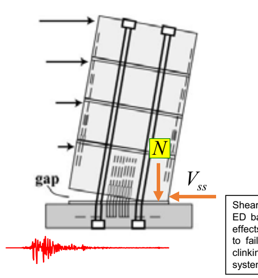

Shear slip failure

$V_{b,\max} > V_{ss}$

$$V_{ss} = \mu_s (A_s f_{sy} + A_p f_p + N_{wb}) = \mu_s N$$

$V_{b,\max}$ = Peak base shear force demand under MCE_R-level
μ_s = Design coefficient of friction
A_s = Area of ED bars
f_{sy} = Stress of ED bars
A_p = Area of PT steel
f_p = Stress of PT bars
N_{wb} = Design axial force at base

Shear slip at the wall foundation interface can cause clinking of ED bars and PT strands. Clinking of ED bars will significantly effects its energy dissipation capacity and eventually may lead to failure under repeated cyclic loading. On the other hand, clinking of PT strands can effect the re-centering of the structural system.

The Methodology

Investigate the applicability of most widely used seismic shear amplification formulas (originally proposed for RC shear walls) to calculate the peak base shear demands in post-tensioned hybrid precast walls under both design earthquake (DE) and risk-targeted maximum considered earthquake (MCE_R) level ground motions considering the effect of frequency content of the ground motion and ED steel moment ratio βm

$$\beta_m = M_{ws} / (M_{wp} + M_{mn})$$

M_{ws} = Moment contribution of ED steel
M_{wp} = Moment contribution of PT steel
M_{wn} = Moment contribution of wall design axial load

ED steel moment ratio βm is a measure of relative amount of mild steel and PT steel used in the walls

Buildings Description

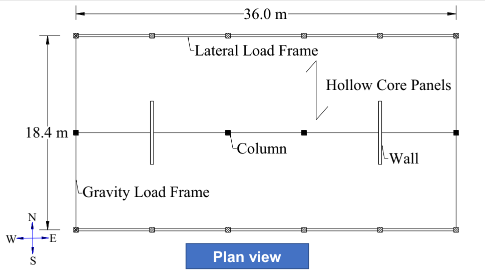

Plan view

- 4-, 8-, 10-, and 12-story walls designed with ED steel moment ratio βm = 0.5 and 0.8.
- Mapped MCE_R spectral response acceleration parameters are S_s = 1.589g, and S_1 = 0.591g at short periods and 1 s period, respectively (similar to Buddika and Wijewickrema 2016).
- Designed using the equivalent lateral force procedure (ELF) following the guidelines given in ACI ITG-5.2 (2009), ASCE/SEI 7 (ASCE 2010), and ACI 318-11 (ACI 2011).

Multi-Spring Macro Model

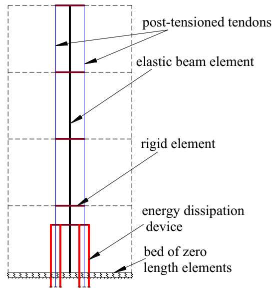

Multi-spring macro model

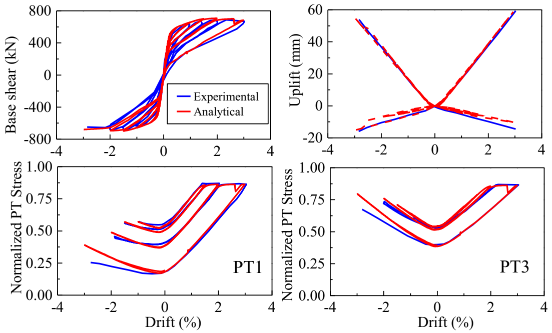

Experiments reported in Perez et al. (2007) were simulated and showed good agreement

Modal Characteristics

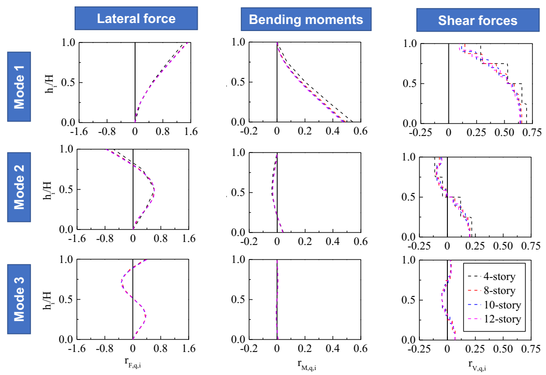

Modal period (s)

Building	Mode 1	Mode 2	Mode 3
4-Story	0.382	0.078	0.030
8-Story	0.739	0.119	0.043
10-Story	0.835	0.134	0.048
12-Story	1.106	0.178	0.064

Modal analysis is carried out, after the gravity load of D + 0.25L (where D is dead load and L is live load) is applied. The ED steel moment ratio βm did not results in a significant changes to their elastic modal characteristics.

Ground Motions and Viscous Damping

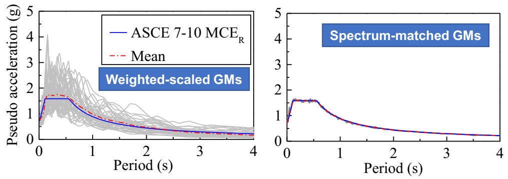

Number of ground motions (GMs)
- Weighted scaling: 40 GMs
- Spectrum matching: 7 GMs

Comparison of 5%-damped response spectra for scaled ground motions with the ASCE 7 MCE_R spectrum.

Tangent stiffness-based Rayleigh damping with a damping ratio ξ = 3% where the damping coefficients are calculated using the first two elastic periods is used

Nonlinear Response History Analysis (NLRHA) Results

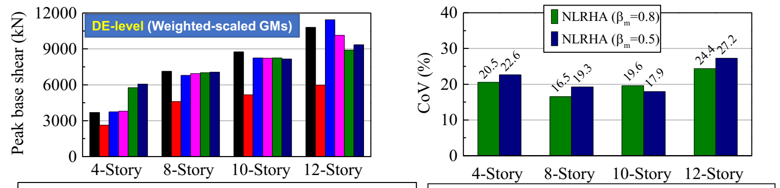

Review of leading code procedures can be found in Rutenberg, A. (2013).

- Peak base shear demands of walls designed ED steel moment ratio βm = 0.5 is comparatively larger than that of walls designed with βm = 0.8.
- Leading code procedures are only satisfactory in estimating peak base shear demands in 8- and 10-story walls

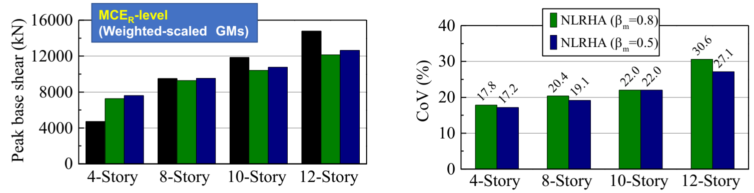

- Most of the shear amplification formulas for RC shear walls are develop considering only DE-level.
- Kurama (1999) procedure is un-conservative for 4-story walls while over-conservative for 12-story walls

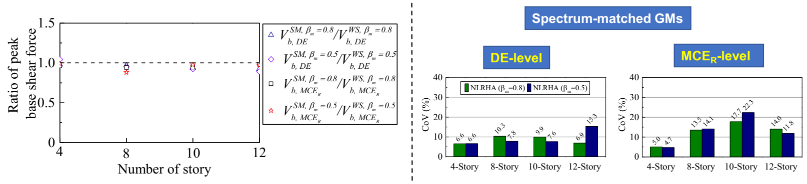

Spectrum-matched ground motions have no significant effect on the estimated peak base shear demands

CoV is comparatively smaller compared to the weighted-scale ground motions

Conclusions

- Leading code procedures are not satisfactory in estimating the peak base shear demands in post-tensioned hybrid precast wall: hence further research is warranted.
- ED steel moment ratio βm = 0.5 results in a comparatively larger base shear demand than that of walls designed with βm = 0.8.
- Spectrum-matched ground motions found to have no significant effect on the estimated peak base shear demands while the coefficient of variation (CoV) is significantly less than compared to that obtained under weighted scaled ground motions

References

Buddika, H. A. D. S., and Wijeyewickrema, A. C. (2016). "Seismic Performance Evaluation of Posttensioned Hybrid Precast Wall-Frame Buildings and Comparison with Shear Wall-Frame Buildings." *J. Struct. Eng.* (ASCE), 10.1061/(ASCE)ST.1943-541X.0001466 , 04016021.
Eberhard, M. O., and Sozen, M. A. (1993). Behavior-based method to determine design shear in earthquake-resistant walls, *J. Struct. Eng.* (ASCE), 119:2, 619-639.
Perez, F. J, Sause, R., and Pessiki, S. (2007). "Analytical and experimental lateral load behavior of unbonded posttensioned precast concrete walls." *J. Struct. Eng.* (ASCE), 133, 1531-1540.
Rutenberg, A. (2013). "Seismic shear forces on RC walls: review and bibliography." *Bull. of Earthquake Eng.*, 11(5), 1727-1751.

DIAPHRAGM ACTION OF SLAB TYPE STRUCTURE CONSISTING OF PRECAST ELEMENTS CONNECTED BY ENERGY DISSIPATERS

STEELab of ITU

INTRODUCTION

In this research, the effects of a group of similar connectors on the overall response of the simple one story precast structures subjected to selected earthquake records have been parametrically investigated. For this purpose, a special structural model has been prepared taking into consideration all kind of material and geometrical nonlinearities and different selected records were used in NLTHA.

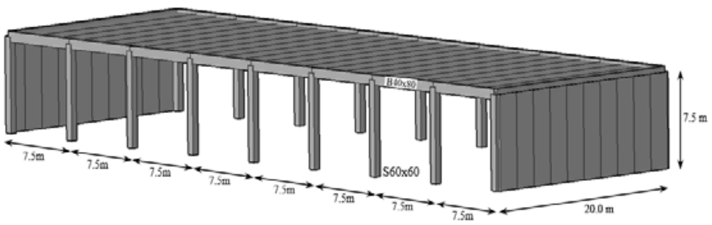

Figure 1. Story plan and features of the building

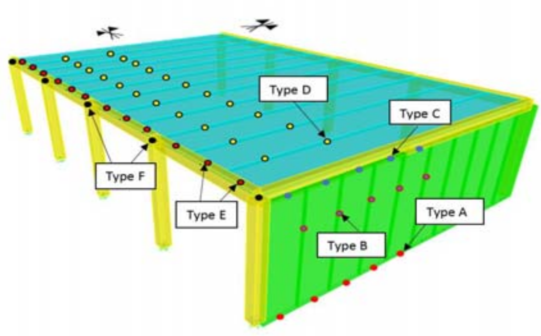

Figure 2 Half of the structural model and designation of connectors

ENERGY DISSIPATIVE CONNECTORS AND THE STRUCTURAL MODEL

Beam to column, beam to cladding, cladding to foundation, cladding to cladding, slab to beam and slab to slab connections (Type A - E) cause drastic changes on the seismic response of the structural building. As connector during parametric analyses, a special type of energy dissipative members named ***steel cushions*** are used which can be utilized for the all connections mentioned above have been developed in the Structural Dynamics and Earthquake Engineering Laboratory of Istanbul Technical University (STEELAB).

The mechanical characteristics of connectors are chosen so that *isolated, integrated and energy dissipative* cladding connections are represented in the model. Since the selected set of parameters of connectors are effective on the free vibrational characteristics of the structure for each analysis *i- periods and mode shapes of the structure, ii- total earthquake energy imparted to the structure, iii- slab in-plane deformations versus rigid diaphragms, iv- energies consumed in each deformed connection* were determined and tabulated for each earthquake records

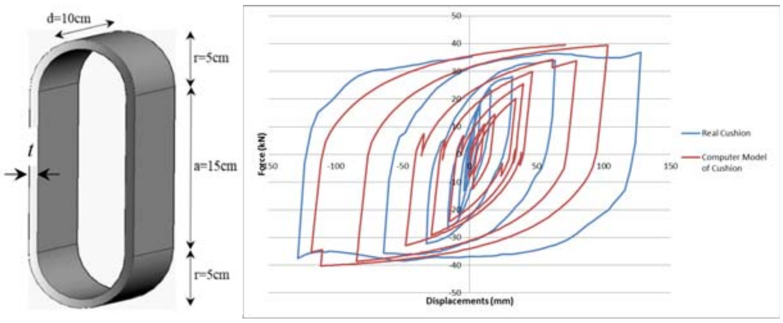

Figure 3. A sample of steel cushion and the experimental out put analytical results

Table 1. Descriptions of Structural Models

Structural Model	Type of Connections				
	A	B	C	D	E
Model 1	SC8	SC5	SC8	I	I
Model 2	SC8	SC5	SC5	I	I
Model 3	SC8	SC5	SC3	I	I
Model 4	DC8	SC5	SC8	I	I
Model 5	DC8	SC5	SC5	I	I
Model 6	DC8	SC5	SC3	I	I
Model 7	SC8	SC5	SC8	SC3	SC8
Model 8	SC8	SC5	SC5	SC3	SC8
Model 9	SC8	SC5	SC3	SC3	SC8
Model 10	DC8	SC5	SC8	SC3	SC8
Model 11	DC8	SC5	SC5	SC3	SC8
Model 12	DC8	SC5	SC3	SC3	SC8

SC8: *Single Cushion (t=8mm),* ***DC8***: *Double Cushion (t=8mm),*
SC5: *Single Cushion (t=5mm),* ***DC5***: *Double Cushion (t=5mm),*
SC3: *Single Cushion (t=3mm),* ***DC3***: *Double Cushion (t=8mm),*
I: Integrated

Table 2. Selected Earthquakes
(Soft Soil – Farfield – 10/50)

NO	Earthquake Name	Scale Factor
No 1	CHICHI03_CHY080-E	0.81498
No 2	CHICHI_CHY006-W	1.012
No 3	NORTHR_LOS270	1.0378
No 4	CHICHI03_TCU076-E	1.0621
No 5	CHICHI_CHY034-N	1.1187
No 6	CHICHI_CHY035-E	1.1293
No 7	CHICHI_CHY006-N	1.1307
No 8	KOBE_KBU000	1.1333
No 9	NORTHR_PKC360	1.1343
No 10	COALINGA_H-Z14000	1.1392
No 11	LOMAP_WVC270	1.1793
No 12	NORTHR_LOS000	1.1805
No 13	HECTOR_HEC090	1.2275
No 14	CHICHI_CHY034-W	1.2494
No 15	CAPEMEND_RIO270	1.2778
No 16	LOMAP_STG000	1.2874
No 17	CHICHI_CHY035-N	1.3106
No 18	LOMAP_CYC285	1.3371
No 19	CHICHI_TCU045-N	1.3752
No 20	LOMAP_G03090	1.3848

Table 3. Energy imparted to the structure and energy dissipated by connectors

DIAPHRAGM	Parameters	Bottom Connection: **Single Cushion**			Bottom Connection: **Double Cushion**		
		Model 1	**Model 2**	**Model 3**	**Model 4**	**Model 5**	**Model 6**
RIGID	T_1 [sec]	0.5398	0.5398	0.5477	0.4262	0.4261	0.5181
	d_i, max [m]	0.028186	0.02812	0.026545	0.023153	0.023439	0.02888
	EI_m [kNm]	233.55	232.84	230.08	207.19	206.61	158.89
	EDRCC [kNm]	21.49	21.28	13.78	6.89	7.73	9.23
	EDRCC/ EI_m (%)	**9.20**	**9.14**	**5.99**	**3.33**	**3.74**	**5.81**
	TED [kNm]	57.83	57.61	60.07	54.98	54.92	38.92
	TED/ EI_m (%)	**24.76**	**24.74**	**26.11**	**26.53**	**26.58**	**24.50**
FLEXIBLE		**Model 7**	**Model 8**	**Model 9**	**Model 10**	**Model 11**	**Model 12**
	T_1 [sec]	0.6174	0.6174	0.6183	0.566	0.566	0.5783
	d_i, max [m]	0.017054	0.017039	0.016789	0.014736	0.014768	0.015718
	EI_m [kNm]	171.53	171.44	168.37	166.10	166.05	166.23
	EDRCC [kNm]	0.03	0.01	0.00	0.00	0.00	0.00
	EDRCC/ EI_m (%)	**0.02**	**0.01**	**0.00**	**0.00**	**0.00**	**0.00**
	TED [kNm]	49.10	49.07	48.05	47.50	47.50	47.46
	TED/ EI_m (%)	**28.62**	**28.62**	**28.54**	**28.60**	**28.60**	**28.55**

T_1: Fundamental period in short direction, ***$d_i$max:*** *Maximum top displacement of NLTHA,* ***EIm*** *: Energy Imparted,*
EDRCC *: Energy Dissipated by Reinforced Concreted Columns,* ***TED*** *: Total Energy Dissipated*

RESULTS

- The fundamental periods in short direction of the structure changes; the more in-plane deformation the longer periods, lower energy imparted, lower displacement demands, are achieved.
- No matter the diaphragm is rigid or flexible, more or less one quarter of the energy imparted to the structure can be dissipated by the proposed connections.
- Selected combinations of connections release that one can design the structure according to preferred energy consumption in the properly chosen energy dissipaters. .
- Ratio of dissipated energy points that the equivalent hysteretic damping ratio will be definitely bigger than five percent which is suggested by most of the codes. The quantification of this will be postponed for the time being.

IRREGULAR SLAB TYPE STRUCTURES CONSISTING OF PRECAST ELEMENTS CONNECTED BY ENERGY DISSIPATERS

STEELab of ITU

INTRODUCTION

Shear walls in short direction at both ends of the classical slab type structures cannot be used for certain structural configurations namely if it has only one or adjacent two exterior sides. When this is the case at a proper one side of the building where shear wall panels can be placed so that tubular parts can be formed with relatively high torsional rigidity using similar cladding panels and connectors in order to resist the big torsional moment due to earthquake forces and to consume a part of the energy imparted to the building.

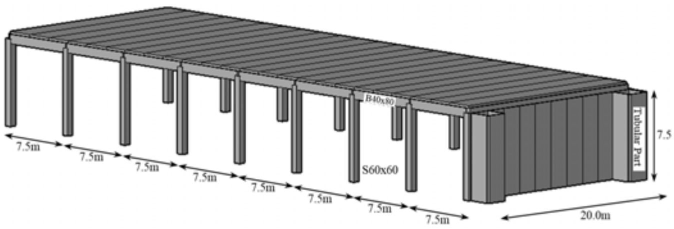

Figure 1. General view of the slab type structure with tubular parts

During the research, the effects of connectors on the overall response of this type irregular simple one story precast structures subjected to selected earthquake records have been parametrically investigated. Special attention has been exercised to see to what extent energy is being dissipated through the special connectors. For this purpose, a structural model has been prepared to carry out plenty of NLTHA taking into consideration all kind of material and geometrical nonlinearities.

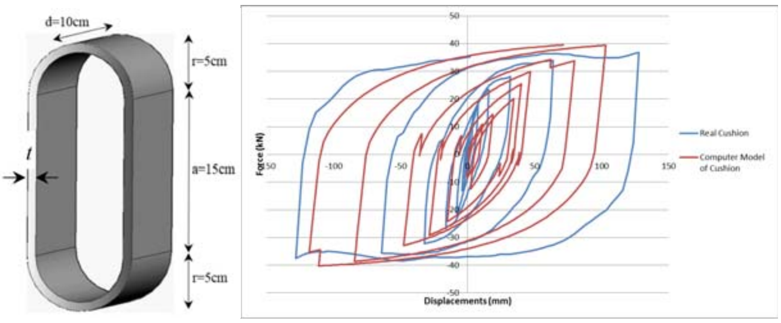

Figure 2. A sample of steel cushion and the experimental out put analytical results

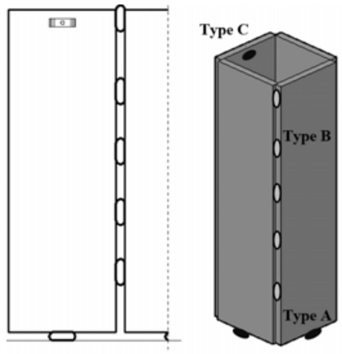

Figure 3 Orientations of steel cushions on claddings and tubular part

ENERGY DISSIPATIVE CONNECTORS AND THE TUBULAR PARTS

A sample of the connectors so called ***steel cushions*** are used which tested in the Structural Dynamics and Earthquake Engineering Laboratory of Istanbul Technical University (STEELAB) more than 100 tests completed choosing different thicknesses, materials, loadings etc. within the framework of the research project called SAFECLADDING which is being supported by European Commission. In this study, connectors are used at the bottom of cladding plates (Type A) and cladding to cladding connection (Type B) of tubular part of system. Connection between tubular part and structural model is designed as very rigid. Since the selected set of parameters of connectors are effective on the free vibrational characteristics of the structure for each analysis *i- periods and mode shapes of the structure, ii- total earthquake energy imparted to the structure, iii-, energies consumed in each deformed connection* were determined .

Table 1. Selected Earthquakes
(Soft Soil – Farfield – 10/50)

NO	Earthquake Name	Scale Factor
No 1	CHICHI03_CHY080-E	0.81498
No 2	CHICHI_CHY006-W	1.012
No 3	NORTHR_LOS270	1.0378
No 4	CHICHI03_TCU076-E	1.0621
No 5	CHICHI_CHY034-N	1.1187
No 6	CHICHI_CHY035-E	1.1293
No 7	CHICHI_CHY006-N	1.1307
No 8	KOBE_KBU000	1.1333
No 9	NORTHR_PKC360	1.1343
No 10	COALINGA_H-Z14000	1.1392
No 11	LOMAP_WVC270	1.1793
No 12	NORTHR_LOS000	1.1805
No 13	HECTOR_HEC090	1.2275
No 14	CHICHI_CHY034-W	1.2494
No 15	CAPEMEND_RIO270	1.2778
No 16	LOMAP_STG000	1.2874
No 17	CHICHI_CHY035-N	1.3106
No 18	LOMAP_CYC285	1.3371
No 19	CHICHI_TCU045-N	1.3752
No 20	LOMAP_G03090	1.3848

Table 2. Descriptions of Structural Models

Model No	Type A	Type B	Type C
MODEL 1	VR	VR	VR
MODEL 2	VR	SC8	VR
MODEL 3	VR	SC5	VR
MODEL 4	VR	SC3	VR
MODEL 5	SC8	SC8	VR
MODEL 6	SC5	SC5	VR
MODEL 7	SC3	SC3	VR
MODEL 8	SC8	SC5	VR
MODEL 9	SC5	SC3	VR

SC8: *Single Cushion (t=8mm),* ***SC5***: *Single Cushion (t=5mm),*
SC3: *Single Cushion (t=3mm),* ***VR*** *: Very Rigid*

Table 3. Energy imparted to the structure and energy dissipated by connectors

		MODEL 1	MODEL 2	MODEL 3	MODEL 4	MODEL 5	MODEL 6	MODEL 7	MODEL 8	MODEL 9
T_1	[sec]	0.4564	0.5043	0.5043	0.5163	0.5077	0.5077	0.5248	0.5077	0.517
EIm	[kNm]	291.31	327.51	314.59	290.20	324.45	323.06	345.65	322.05	277.14
EDRCC	[kNm]	44.56	30.69	31.55	32.91	31.95	31.49	28.35	31.84	32.66
EDRCC/EIm	[%]	**15.30**	**9.37**	**10.03**	**11.34**	**9.85**	**9.75**	**8.20**	**9.89**	**11.78**
EDC	[kNm]	0.00	26.32	30.16	5.73	25.97	26.01	36.96	26.21	9.99
EDC/EIm	[%]	**0.00**	**8.04**	**9.59**	**1.97**	**8.00**	**8.05**	**10.69**	**8.14**	**3.60**
TED	[kNm]	71.70	83.45	81.20	70.64	82.55	82.01	83.80	82.24	67.87
TED/EIm	[%]	**24.61**	**25.48**	**25.81**	**24.34**	**25.44**	**25.39**	**24.25**	**25.54**	**24.49**

T_1: Fundamental period in short direction, ***EIm*** *: Energy Imparted,*
EDRCC: *Energy Dissipated by Reinforced Concreted Columns*
EDC *: Energy Dissipated by Steel Cushions* ***TED*** *: Total Energy Dissipated*

RESULTS

- The flexibility provided to the structure by energy dissipating connectors increases the chance of a proposal for a cost effective design procedures not only for retrofitting of the existing industrial buildings but also for new constructions.
- Hysteretic energy dissipated at each connection indicates to what extent effective will be the connector used in that particular location. This is going to be a chance for having adopted the concept of energy based design for retrofitting the existing precast buildings and new precast simple structures.
- The demand of torsional resistance of this type irregular structure is reduced by using special energy dissipating connectors between slab and cladding elements for controlled transfer of the inertia forces to the foundation system.

CYCLIC TEST of the PRECAST PANELS EQUIPPED with STEEL CUSHIONS

STEELab of ITU

The site observations on the severely damaged precast buildings after the L'Aquila Earthquake (2009) demonstrated that the connecting details in between the claddings and the precast RC members are extremely effective on the overall earthquake behaviour of the precast structure. **SAFECLADDING** a new research study, has been initiated in the scope of FP7 research project aiming to evaluate the earthquake performance of the existing connections for RC cladding systems and aiming to develop an innovative steel devices accumulated through the interface of the claddings with the RC members.

Figure 1: General Views of Testing Set Up

A brand new low-cost steel cushion has been developed in the Structural and Earthquake Engineering Laboratory of ITU to be used in the connections of cladding systems. A fully pinned (pin jointed) swaying steel frame transferring the lateral loads to the precast panel system over the accumulated steel cushions, has been designed and produced in the laboratory as a preparation for the experimental part of SAFECLADDING Project. The testing set-up is composed of four RC precast panels with the dimensions of 1.0 × 2.5 m are located in the pin jointed steel frame simultaneously. In this study, steel cushions with thickness of 5 mm are attached to the panel to panel, 3 mm thick specimen is attached to panel to foundation connections and 8 mm thick cushions are located trough the beam to panel connections. The experimental results are discussed and compared in terms of load displacement hysteresis curves and dissipated cumulative energies.

Figure 2: Precast Panels **without** Steel Cushions (Test I)

Figure 3: Precast Panels **with** Steel Cushions (Test II)

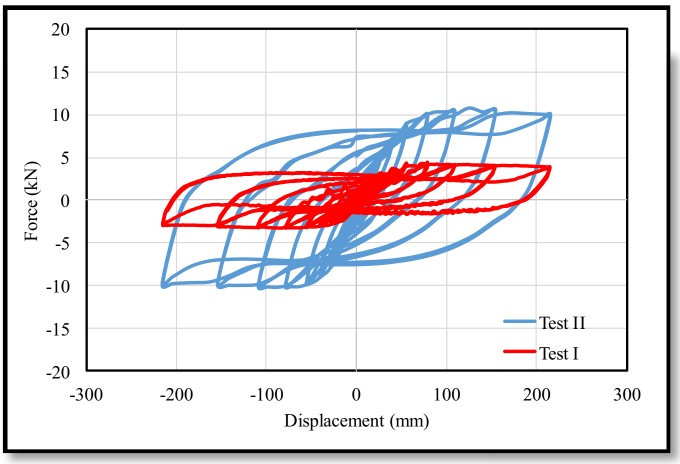

Figure 4: Force-Displacement Hysteresis Comparison

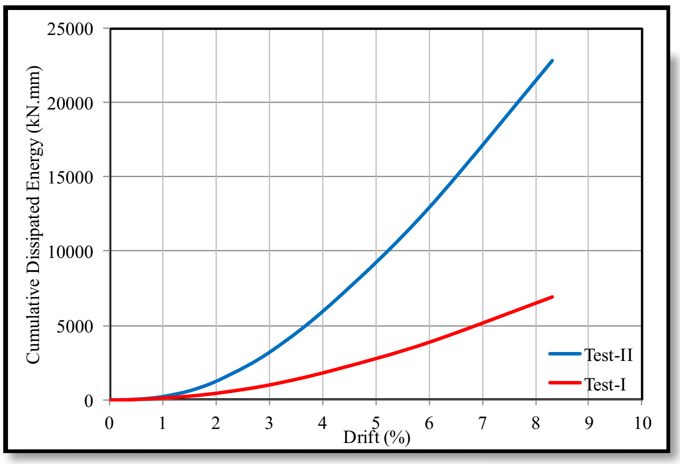

Figure 5: Cumulative Dissipated Energy Comparison

In conclusion it is foundout that 5 mm thick steel cushion is agreat source of energy dissipation when it is accumulated through the interface of the RC cladding panels used in precast structures.

ANALYTICAL and NUMERICAL STUDIES on the ENRGY DISSIPATIVE STEEL CONNECTORS

STEELab of ITU

Analytical and numerical studies were conducted on the energy dissipative steel connectors which initially were developed and experimentally investigated in the Structural and Earthquake Laboratory of Istanbul Technical University in the scope of SAFECLADDING project founded by FP7. The aim of these studies were to extract the closed formed equations to predict the yielding and post yielding properties of the energy dissipative steel connectors with different geometrical characteristics without any need to extra experiments. The analytical studies were implemented with the finite element program ABAQUS.

Finite Element Model

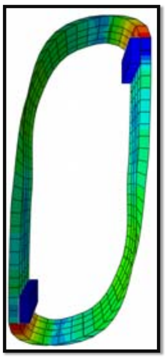

Deformed shape (Shear Loading)

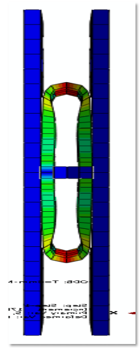

Deformed shape (Compression Axial Loading)

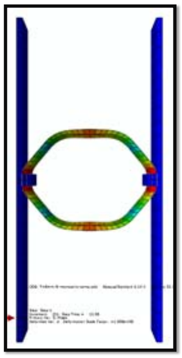

Deformed shape (Compression Axial Loading)

Figure 1: Finite Element Model of the Energy Dissipative Steel Connectors

The energy dissipative steel connectors with three distinct thicknesses of 3mm, 5mm and 8mm were modelled in the ABAQUS program and the analytical model was calibrated with the experimental results, finally the closed formed equation was validated with the analytical results. The closed-form equations were derived through the classical Force method.

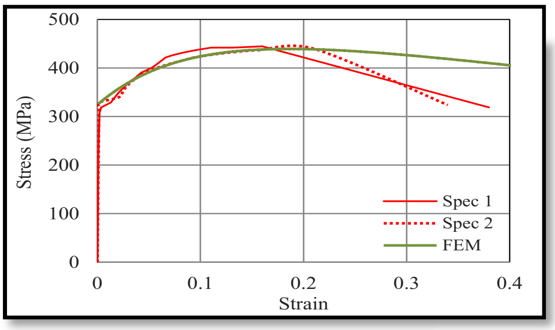

ABAQUS simulation of steel coupon tests

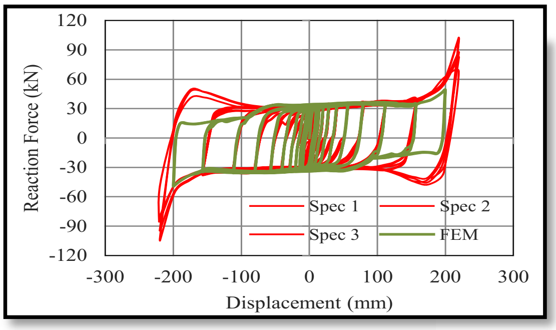

Cyclic shear force vs. displacements

Figure 2: Comparison of Experimental and Analytical results

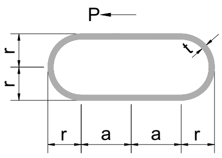

Work of axial and shear deformations will be neglected	
Moment	$M(\phi)=\frac{\mathrm{Pr}}{2}(1-\cos\varphi)+\frac{a+r\sin\varphi}{r+a}\left[-\frac{\mathrm{Pr}(a+r)(a^2+\pi ar+2r^2)}{(4/3)a^3+2\pi a^2r+8ar^2+\pi r^3}\right]$ $M_{\max}=M(\varphi_{\max})$
Location of Max. Moment	$\phi_{\max}=-\frac{1}{2}\log\left(\frac{1.5i\pi r^3+12iar^2-3a^2r+2ia^3-6r^3-3\pi ar^2+3i\pi a^2r}{1.5i\pi r^3+12iar^2+3a^2r+2ia^3+6r^3+3\pi ar^2+3i\pi a^2r}\right)i$
Longitudinal Displacement	$\delta_h=\frac{Pr^2}{EI}\left(\frac{5a^4+9\pi a^3r+(36+1.5\pi^2)a^2r^2+12\pi ar^3+(2.25\pi^2-12)r^4}{4a^3+6\pi a^2r+24ar^2+3\pi r^3}\right)$

Figure 3: Drived Closed-Form Equation for Shear Loading

In conclusion the extracted closed-form equation is provided the ease for the structural engineers to estimate the required properties of the energy dissipative connectors in the practice with high accuracy under the shear and axial stresses.

1st Joint Workshop

Japan-Turkey Cooperative Program on Resilience Engineering for Energy and Urban Systems

İstanbul, February 2016

MODELLING HYSTERETIC BEHAVIOUR OF U-SHAPED STEEL DAMPERS

Kurtuluş Atasever *

Prof. Oğuz Cem Çelik **, Assos. Prof. Ercan Yüksel **

***Mimar Sinan Fine Arts University, **Istanbul Technical University**

INTRODUCTION

Building structures are subjected to variable loads (wind, earthquake, snow etc.) many times during their lifetime. Among these effects, earthquake loading usually creates the worst conditions for structures, because during an earthquake input energy, which reaches structural elements, may cause cracks and other types of the heavy structural damage. Conventional approach to earthquake resistant building design (ERBD) relies upon strength, stiffness and inelastic deformation capacity, which are great enough to withstand a given level of earthquake effects. However, modern approach in today's designs aims to reduce/mitigate seismic energy before the input energy reaches the structural elements. As a structural and damage control technology for buildings, seismic isolation systems reduce forces, by shifting the natural period of structure away from the dominant period of earthquake excitation. On the other hand, energy-dissipating systems provide damping for seismic input energy. A design approach, uses both of the systems together, is known as the modern design approach.

DAMPER AND MATERIAL MODELLING

In order to simulate hysteretic behavior under lateral loads, a 3D finite element model (FEM) of UD is developed with ABAQUS. Two type of steel material Q235 and SN490B are used and UD dampers analyzed under three different load protocol.

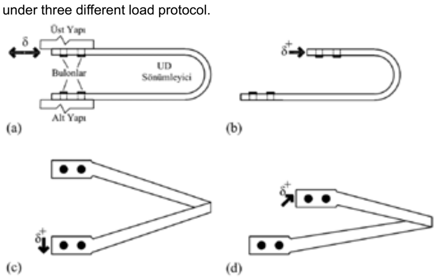

Figure 1: Various Loading Directions

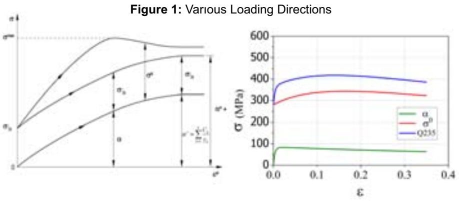

Figure 2: (a) One dimensional represantation of combined material model (b) Hardening parameters of Q235 Steel Material

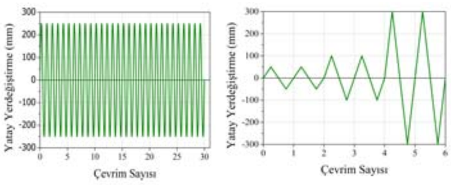

Figure 3: Load Protocols

VERIFICATION OF FEM MODEL

Finite Element Model was adopted for UD40 damper, which has an experimental study on it. This opportunity made it possible to compare experimental and FEM results. It was observed that both permanent deformations and hysteretic behavior under lateral loads, which were determined from FEM analysis, are similar to experimental results. Deformations on UD40 under 0 degree was mainly caused by cyclic bending in the dampers, which was concentrated mostly in the middle part of the upper and lower arms. However, the deformations on UD40 under 90 degrees cyclic loading was mostly caused by the torsion and concentrated at the end of the damper arm near the connections.

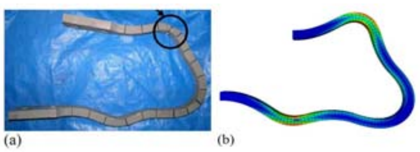

Figure 4: 0 Degree (a) Experimental Result (Jiao et al 2015) (b) Numerical Result

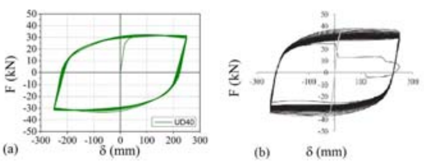

Figure 5: 0 Degree (a) Numerical Hysteretic Curve (b) Experimental Hysteretic Curve (Jiao et al 2015)

NUMERICAL EXAMPLES AND ANALYSIS RESULTS

It is known that hysteretic behavior of UD devices varies with changing geometry of the damper. For this reason, designing UD damper's geometry for any seismic demand would be quite important. Total of 10 new dampers (two different types) are geometrically designed and their hysteretic behaviors are compared.

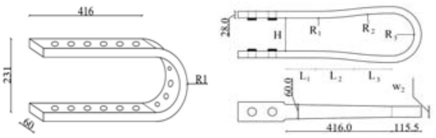

Figure 6: Typical Shapes (a) UDK (b) UDF Geometry

UDF is formed by bending of upper and lower arms to obtain axial forces by minimizing bending effects. UDK is formed by opening holes along the arms. At same cycle number, UDF mostly dissipated more energy than UD40. Plastic deformations on UDF dampers concentrated between bended arms and curved plate. UDK had lower first effective stiffness than UD40. Deformations on UDK dampers concentrated around biggest hole and this hole controlled behavior of UDK dampers. Therefore, it must be chosen around 20 mm (R/t=0.28) hole diameter in order to distribute plastic deformations. All UD damper's effective damping ratio was determined more as 50 percent or above. UD dampers have similar hysteretic behavior under any loading direction. In practice, these dampers are used as a combined system instead of a single part. Therefore, in this study hysteretic behavior of UD systems are also investigated under different loading directions.

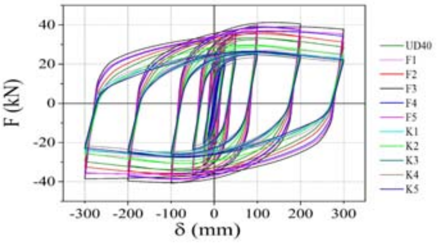

Figure 7: Comparison of Hystertic Curves

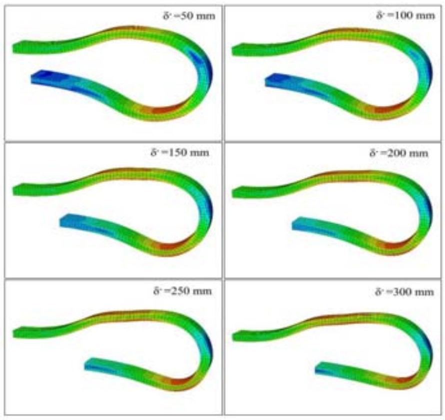

Figure 8: Stress and Deformations Distribution

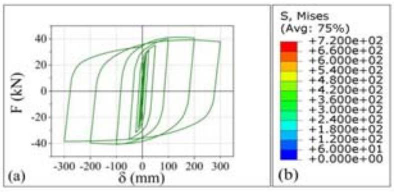

Figure 9: (a) Hysteretic Curve (b) Legant

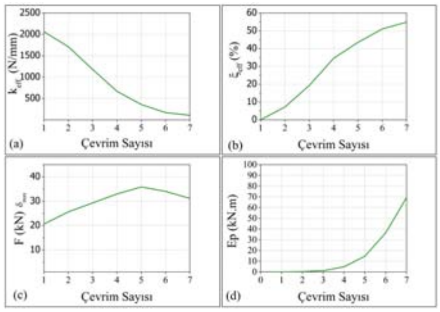

Figure 10: (a) Effective Stiffness (b) Effetive Damping (c)Forces at Maximum Displacement (d) Cumulative Dissipated Energy

Table 1: Comparison of Dampers Performance (0 Degree 7 Cycle)

	UD40	UDF1	UDF2	UDF3	UDF4	UDF5
Y	12.5 mm	15 mm	10 mm	7.5 mm	10 mm	10 mm
PEEQ	0.27	0.28	0.35	0.50	0.43	0.43
σ_{maks}	591.7 MPa	577.9 MPa	604.5 MPa	651.4 MPa	644.4 MPa	645.7 MPa
Plastic Strain Concentration	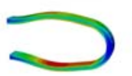					
$k_{eff}/k_{eff(UD40)}$	1.00	0.69	1.21	1.45	1.38	1.40
$Ep/Ep_{(UD40)}$	1.00	0.79	1.09	1.25	1.17	1.19
$\xi_{(1.\ Çevrim)}$	%0	%0	%0	%5	%2	%3
	UD40	**UDK1**	**UDK2**	**UDK3**	**UDK4**	**UDK5**
Y	12.5mm	7.5mm	10mm	10mm	10mm	7.5mm
PEEQ	0.27	1.66	0.429	0.740	1.06	1.174
σ_{maks}	591.7 MPa	723 MPa	640.7 MPa	683.2 MPa	714.4 MPa	718.4 MPa
Plastic Strain Concentration	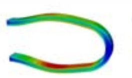					
$k_{eff}/k_{eff(UD40)}$	1.00	0.80	0.88	0.81	0.77	0.78
$Ep/Ep_{(UD40)}$	1.00	0.77	0.87	0.79	0.74	0.77
$\xi_{(1.\ Çevrim)}$	%0	%2	%0	%0	%0	%1

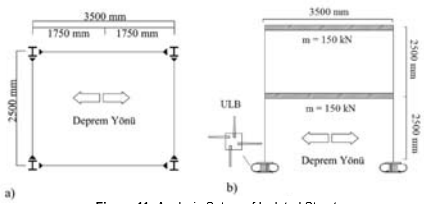

Figure 11: Analysis Set up of Isolated Structure

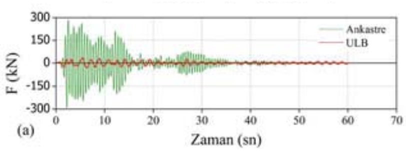

Figure 12: Base Shear 18 May 1940 El Centro

NONLINEAR ANALYSIS OF AN ISOLATED STRUCTURE

To further investigate real behavior of ULB as base isolation system under real ground motions, four earthquake ground motion data were used. To this end, a two-story structural system was modelled with structural analysis program SAP2000, as fixed base and isolated base. 18 May 1940 El Centro, 17 January 1994 Northridge, 31 October 1935 Helena Montana and 17 August 1999 Kocaeli ground motions were used for this analysis model. According to fast nonlinear analysis (FNA) results, under large displacements of the structure implementation of ULB resulted in a large decrease in maximum base shear forces and story drifts.

CONCLUSIONS

According to the analysis results obtained here stable hysteretic behavior can be achieved for UD and this would improve largely the seismic performances of structures. In addition to this, as this system seems a low-cost seismic device, it is possible to manufacture such devices with the help of local producers in Turkey. This would result in a widespread use of seismic isolation systems in existing and new buildings located seismically vulnerable areas.

REFERENCES: Atasever, K. (2016). *Modellıng hysteretıc behavıour of U-shaped steel dampers and usıng such dampers wıth low dampıng rubber bearıngs as seısmıc isolator.* MSc. Istanbul Technical University.

UNIAXIAL and BI-DIRECTIONAL TESTS of the ENRGY DISSIPATIVE STEEL CONNECTORS

STEELab of ITU

Past experiences acquired after strong ground motions such as L'Aquila Earthquake (2009) clearly demonstrated the deficiency of the connectors in panel to beam elements in terms of strength and ductility in the precast concrete industrial buildings. To resolve these problems and to improve the performance of the precast concrete industrial buildings under the dynamic excitation a novel oval-shaped energy dissipative steel connector was developed and experimentally investigated in the Structural and Earthquake Laboratory of Istanbul Technical University in the scope of SAFECLADDING project founded by FP7.

Shear Test

Axial Test

Bi-Directional Test under Combination of Shear and Axial Loading

Figure 1: Uniaxial and Bi-Directional Tests on the Energy Dissipative Steel Connectors

The innovative energy dissipative connectors with three distinct thicknesses of 3mm, 5mm and 8mm were tested under various loading such as shear, axial effect and combination of the shear and axial loading and their elastic and post-elastic behaviour were determined. In the Bi-Directional tests the shear response of the energy dissipater steel connectors were obtained under different level of the tensile and compression axial loading individually.

.

Shear Test

Compression Axial Test

TensionAxial Test

Shaer and Compression Axial Test

Shaer and TensionAxial Test

Figure 2: Deformed Shape of the Energy Dissipative Steel Connectors

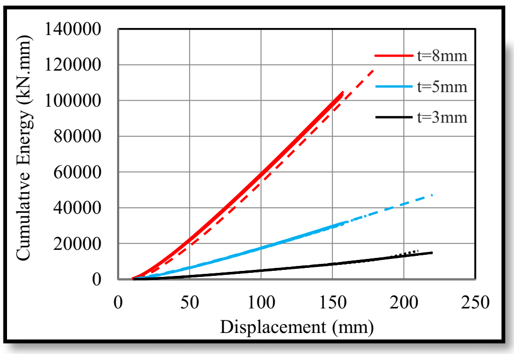

Cumulative Damping vs. Displacement (Shear Test)

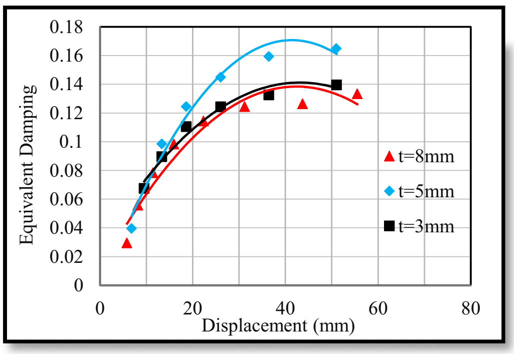

Equivalent Damping Ratio vs. Displacement (Axial Test)

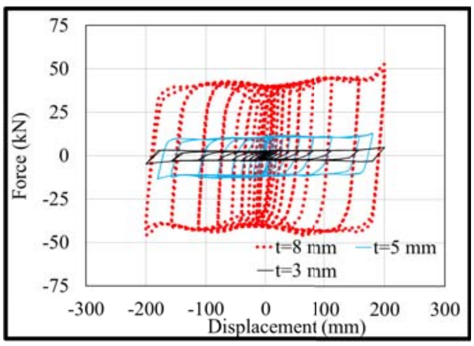

Force vs. Displacement (compression Axial and Shear Test)

Figure 3: Experimental Results obtained from Uniaxial and Bi-Directional Tests

The results show that the energy dissipative steel connector can be a considerable source of energy dissipation during the seismic excitation also the force displacement hysteresis are stable and the steel connectors have significant displacement capacity up to 220 mm under the shear action. Moreover the direction of the axial loads and their intensity are effective in the yielding and post-yielding behavior of steel connectors.

Axial Behavior of Prismatic HPFRCC Externally Confined by CFRP Sheets

Ugur Demir, Yusuf Sahinkaya, Medine Ispir and Alper Ilki

Istanbul Technical University, Structural Engineering Department

Abstract

This poster presents the results of the axial behavior of high performance fiber reinforced cementitious composites (HPFRCC) confined by FRP sheets. Experimental results and ultimate behavior such as ultimate strength and strains are reported . At the second half, model performances on predicting the ultimate behavior were investigated and a new unique model is proposed. The proposed model was the best in aggreement with the experimental data.

Introduction and Background

HPFRCC behavior is defined as linear elastic under compression (JSCE, 2008). Some researchers reported that relatively ductile behavior of HPFRCC mostly depends on the composition and content of the composite in some cases leads to less ductile behavior (Li and Liu 2012). FRP confinement of HPFRCC can be promising for achieving ductile failure mechanisms in axially loaded structural members. This poster presents experimental investigation carried out on 20 prismatic specimens with square and rectangular shapes. The performances of 10 existing models applicable to FRP confined conventional concrete were assessed in predicting the ultimate behavior. Finally, a unified model, to predict the ultimate behavior of FRP confined prismatic HPFRCC columns was developed based on the experimental data of the presented study. The proposed model was better than any of investigated models in agreement with the experimental data.

Methods

A total of 20 HPFRCC, including 6 square and 10 rectangular specimens confined by carbon fiber reinforced polymer (CFRP) jackets of various axial rigidities and 2 unconfined specimens for each cross-section were manufactured and then tested under uniaxial compressive loading. Cross sectional dimensions were 150 mm x 150 mm for square specimens and 150 mm x 225 mm for rectangular ones. All specimens had the height of 300 mm. Mix proportion of the HPFRCC is given in Table 1. As seen in Fig. 1, for measuring the axial deformations, 2 linear variable differential transformers with a measurement capacity of 25 mm (LVDT-25) were mounted.

Table 1: HPFRCC Mix proportions of cementitious composite (kg/m^3)

C	SF	S	STF	W	SP	Total
1000	250	815	78.5	124	125	2392.5

Fig. 1 Test set-up and instrumentation

Experimental Results and Discussion

As seen in Tables 2 and 3; for square specimens, confined with two to ten layers of CFRP, ultimate axial strength was enhanced by 15 to 22%, while ultimate axial strain was improved by 157 to 570%. For rectangular columns confined with two to ten layers of CFRP, ultimate axial strength was enhanced by 13 to 37% and the ultimate axial strain was improved by 317 to 555%. For rectangular specimens, confined with 12 plies of FRP, axial strength was enhanced by 48%, while ultimate axial strain was improved by 548%.

Analytical Results

A new design oriented model to predict the ultimate condition of CFRP confined prismatic HPFRCCs is proposed based on experimental findings (Eqs.1 and 2). Comparison of predictions with some of the other available models in the literature shows that, proposed model gives the most satisfactory results. For the proposed model, evaluated *AAE* values in predicting ultimate strength and strain values are 0.06 and 0.08 while the *SD* values are 0.07 and 0.13, respectively.

$$\frac{f'_{cc}}{f'_{co}} = 1 + 1.71\frac{f'_{l,\max}}{f'_{co}} \quad (1) \qquad \frac{\varepsilon_{cc}}{\varepsilon_{co}} = 2 + 23\frac{f'_{l,\max}}{f'_{co}} \quad (2)$$

Table 2: Experimental Test Results for Square Specimens

Specimen00	f'_{co} (MPa)	f'_{cc} (MPa)	ε_{co}	ε_{cu}	$\varepsilon_{h,rup}$	f'_{cc}/f'_{co}	$\varepsilon_{cu}/\varepsilon_{co}$	Average f'_{cc}/f'_{co}	Average $\varepsilon_{cu}/\varepsilon_{co}$
CC-S-0-1	102.2	x	0.0035	x	0.001	x	x	x	x
CC-S-0-2	110.6	x	0.0036	x	0.001	x	x		
CC-S-2-1	x	122.0	x	0.0096	0.005	1.15	2.67	1.15	2.57
CC-S-2-2	x	121.8	x	0.0089	0.005	1.14	2.47		
CC-S-8-1	x	120.9	x	0.0173	0.005	1.14	4.81	1.22	4.73
CC-S-8-2	x	138.3	x	0.0167	0.004	1.30	4.64		
CC-S-10-1	x	137.6	x	0.0259	0.007	1.30	7.20	1.22	6.70
CC-S-10-2	x	121.2	x	0.0223	0.006	1.14	6.19		

Table 3: Experimental Test Results for Rectangular Specimens

Specimen	f'_{co} (MPa)	f'_{cc} (MPa)	ε_{co}	ε_{cu}	$\varepsilon_{h,rup}$	f'_{cc}/f'_{co}	$\varepsilon_{cu}/\varepsilon_{co}$	Average f'_{cc}/f'_{co}	Average $\varepsilon_{cu}/\varepsilon_{co}$
CC-R-0-1	95.8	x	0.0027	x	0.001	x	x	x	x
CC-R-0-2	92.5	x	0.0033	x	0.002	x	x		
CC-R-2-1	x	106.0	x	0.0125	0.004	1.13	4.17	1.13	4.17
CC-R-2-2*	x	82.3	x	0.0117	0.005	0.87	3.90		
CC-R-6-1	x	132.1	x	0.0152	0.004	1.40	5.07	1.39	4.55
CC-R-6-2	x	130.2	x	0.0121	0.004	1.38	4.03		
CC-R-8-1	x	113.3	x	0.0145	0.006	1.20	4.83	1.35	5.47
CC-R-8-2	x	140.9	x	0.0183	0.005	1.50	6.10		
CC-R-10-1	x	131.9	x	0.0196	0.004	1.40	6.53	1.37	6.55
CC-R-10-2	x	125.5	x	0.0197	0.004	1.33	6.57		
CC-R-12-1	x	140.9	x	0.0197	0.005	1.50	6.57	1.48	6.48
CC-R-12-2	x	137.9	x	0.0192	0.005	1.46	6.40		

References

Brandt, A. M. (2008). Fiber reinforced cement-based (FRC) composites after over 40 years of development in building and civil engineering. *Composite structures, 86(1), p. 3-9.*

Li, Y. and Liu, Z. J. (2012), Behavior of High Performance PVA Fiber Reinforced Cement Composites under Uniaxial Compressive Load. *Applied Mechanics and Materials 174, p. 687-691).*

Japan Society of Civil Engineers (JSCE) Concrete Engineering (2008), Recommendations for design and construction of high performance fiber reinforced cement composites with multiple fine cracks (HPFRCC).

Seismic Intensity Maps for Scenario Events on the Eastern Segments of North Anatolian Fault Zone of Turkey based on Simulated Ground Motion Data

Shagahyegh Karimzadeh (shaghayegh.karimzadehnaghshineh@metu.edu.tr)

Aysegul Askan (aaskan@metu.edu.tr), Mustafa Bilal (mst.bilal@gmail.com)

I. Abstract: Seismic intensity maps represent the effects of an earthquake on the Earth's surface and generally contribute in rapid assessment in the aftermath of earthquakes. Digital intensity maps employ correlations between felt intensity and peak ground motion values. The purpose of this study is to present spatial distribution of macroseismic intensities in terms of modified Mercalli (MMI) scale, across the North Anatolian Fault Zone (NAFZ) in Turkey. In comparison to the western segments of NAFZ, eastern parts have been less studied and also have sparse ground motion networks. Thus, in this study, MMI distributions of potential scenario events are studied on the eastern segments of NAFZ through ground motion simulations. In particular, the study region is considered to be Erzincan which is a small city in eastern of Turkey, located in the conjunction of three active faults: North Anatolian, North East Anatolian and Ovacik Fault Zones. Erzincan city center is in a pull-apart basin underlain by soft sediments which considerably amplify the ground motions. Combination of the tectonic and geological settings of the area have resulted in catastrophic events such as the 27 December 1939 (Ms=8.0) and the 13 March 1992 (Mw=6.6) earthquakes leading to major losses. In this study, initially ground motion simulations for a set of scenario events as well as the 1992 Erzincan earthquake (Mw=6.6) are performed. Then, to assess the corresponding MMI values, recently-derived local relationships between MMI and PGA as well as PGV are employed. The final results are expressed in the form of digital intensity maps for the 1992 event and the scenario earthquakes.

II. Study Region: Erzincan

- Built on an alluvium pull-apart basin (50 km x 15 km)
- Located in the conjunction of three active faults: North Anatolian, North East Anatolian and Ovacik Faults
- Experienced destructive earthquakes: the 1939 event (Ms=8.0); the 1992 event (Mw=6.6)
- An active right-lateral strike-slip fault
- Has sparse seismic networks
- Only 3 stations recorded the 1992 event

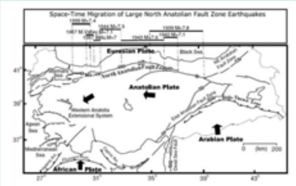

Figure 1. Major tectonic structures around the Anatolian plate

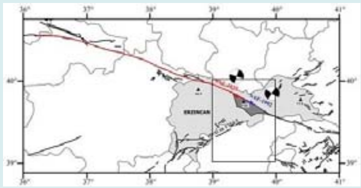

Figure 2. Seismotectonics in the Erzincan region with the fault systems and the epicenters of the 1939 and 1992 events

III. Ground Motion Simulation Methodology and Results of Simulations along Eastern Segments of NAFZ:

Method of simulation: Stochastic Finite Fault Method: (Motazedian and Atkinson, 2005)

- Rectangular fault plane subdivided into subfaults of stochastic point sources
- Subsource contributions are summed in time domain

Ground motion Simulations along Eastern Segments of NAFZ:

- The 1992 event is simulated
- Simulation of scenario earthquakes with: Mw=6.0; Mw=6.5; Mw=7.0
- For all scenarios: using the same epicenter of the 1992 Erzincan event (Mw=6.6)
- Selecting the source, path and site parameters introduced by Askan et al. (2013) : validated for mainshock of the 1992 event
- Simulations within EXSIM program

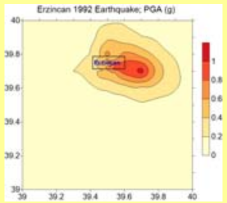

Figure 3. Spatial distribution of the simulated PGA values of the 1992 Erzincan earthquake

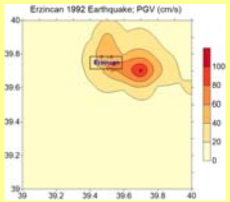

Figure 4. Spatial distribution of the simulated PGV values of the 1992 Erzincan earthquake

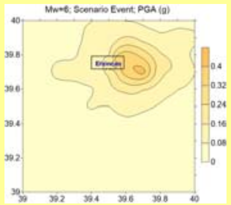

Figure 5. Spatial distribution of the simulated PGA values of the of the scenario earthquake with Mw=6

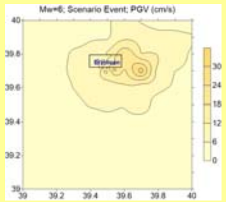

Figure 6. Spatial distribution of the simulated PGV values of the scenario earthquake with Mw=6

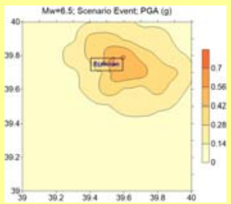

Figure 7. Spatial distribution of the simulated PGA values of the scenario earthquake with Mw=6.5

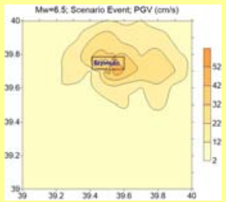

Figure 8. Spatial distribution of the simulated PGV values of the scenario earthquake with Mw=6.5

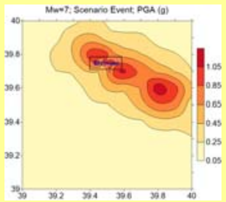

Figure 9. Spatial distribution of the simulated PGA values of the scenario earthquake with Mw=7

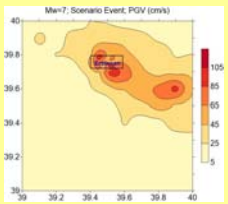

Figure 10. Spatial distribution of the simulated PGV values of the scenario earthquake with Mw=7

IV. Relationships between Peak Ground Motion Parameters and Felt Intensity Values:

To assess the spatial distribution of potential seismic damage:

•Using the local correlations of Bilal and Askan, (2014)

•Correlations between: measured ground motion parameters (PGA and PGV) and felt intensity values in terms of modified Mercalli (MMI) scale

$$MMI = 0.132 + 3.884\log(PGA) \quad \text{(Equation1)}$$

$$MMI = 2.673 + 4.340\log(PGV) \quad \text{(Equation2)}$$

V. Applications in the Study Region:

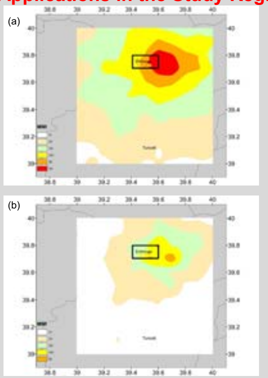

Figure 11. Digital intensity map of the scenario event with Mw=6.0 using (a) Equation (1), (b) Equation (2)

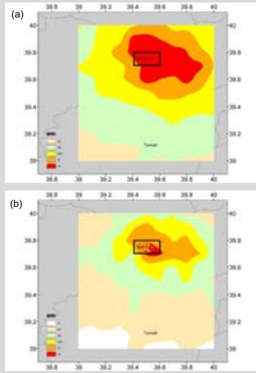

Figure 12. Digital intensity map of the scenario event with Mw=6.5 using (a) Equation (1), (b) Equation (2)

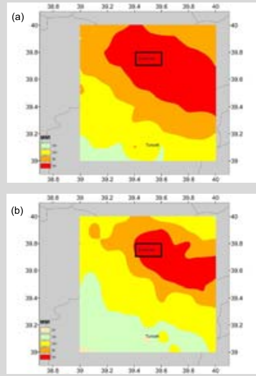

Figure 13. Digital intensity map of the scenario event with Mw=7.0 using (a) Equation (1), (b) Equation (2)

VI. Conclusions:

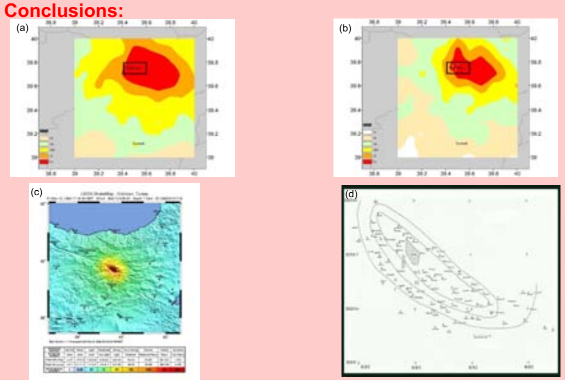

Figure 13 Comparison of the felt intensity map of the 1992 Erzincan earthquake in terms of MMI scale (a) obtained using the MMI-PGA correlation given in Equation (1), (b) obtained using the correlation given in Equation (2), (c) prepared by the USGS ShakeMap software, (d) prepared in the field by Turkish Ministry of Construction in 1992 ((c) is adapted from http://earthquake.usgs.gov/earthquakes/shakemap/atlas/shake/199203131718/)

VII. References:

Askan A., Karimzadeh S. , and Bilal M. (2016). Seismic intensity maps for North Anatolian Fault Zone (Turkey) based on recorded and simulated ground motion data, Book Chapter, Neotectonics and Earthquake Potential of the Eastern Mediterranean Region, AGU Books.

Askan, A., Sisman, F.N., and Ugurhan, B. (2013). Stochastic strong ground motion simulations in sparsely-monitored regions: A validation and sensitivity study on the 13 March 1992 Erzincan (Turkey) earthquake, Soil Dynamics and Earthquake Engineering, 55, 170-181.

Bilal M. and Askan A. (2014). Relationships between Felt Intensity and Recorded Ground-Motion Parameters for Turkey, Bulletin of the Seismological Society of America, Vol. 104, No. 1, 2014, doi: 10.1785/0120130093.

Selection Of Steam Turbine Types In Thermal Power Plants

Fatih AVCI
Mechanical Engineer

Energy Institute
Energy Science & Tech. MSc. Program

Steam turbine is the prime mover which transformed steam potential energy into kinetic energy. Then this kinetic energy rotates shaft and generate mechanical energy. It is the turbine that used in Rankine Cycle.

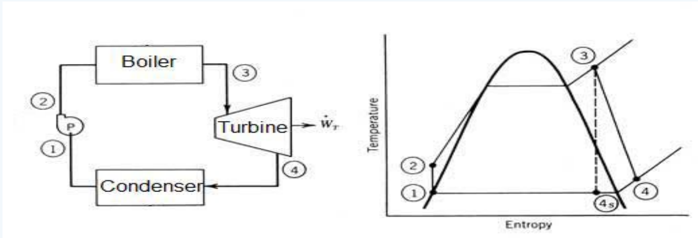

$$W_{turbine} = h_3 - h_4 \qquad \eta = \frac{h_3 - h_{4s}}{h_3 - h_4}$$

Steam turbine types, according to action of steam;

- **Impulse Turbine :** In impulse turbine, steam coming out through a fixed nozzle at a very high velocity strikes the blades fixed on the periphery of a rotor. The blades change the direction of steam flow without changing its pressure. The force due to change of momentum causes the rotation of the turbine shaft.

- **Reaction Turbine :** In reaction turbine, steam expands both in fixed and moving blades continuously as the steam passes over them. The pressure drop occurs continuously over both moving and fixed blades.

- **Combination of Impulse and Reaction**

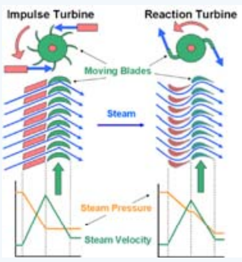

Steam turbine types, according to heat drop process;

- **Condensing turbines** : In these turbines, steam at a pressure less than the atmospheric is directed to the condenser. The steam is also extracted from intermediate stages for feed water heating). The latent heat of exhaust steam during the process of condensation is completely lost in these turbines.
- **Condensing turbines with one or more intermediate stage extractions:** In these turbines, the steam is extracted from intermediate stages for industrial heating purposes.
- **Back pressure turbines:** In these turbines, the exhaust steam is utilized for industrial or heating purposes. Turbines with deteriorated vacuum can also be used in which exhaust steam may be used for heating and process purposes.
- **Topping turbines:** In these turbines, the exhaust steam is utilized in medium and low pressure condensing turbines. These turbines operate at high initial conditions of steam pressure and temperature, and are mostly used during extension of power station capacities, with a view to obtain better efficiencies.

In power plants, the turbine type is getting important because of the electricity prices against process steam prices. The electricity prices are become crucial for thermal power plants operation. The feed-in tariff on electricity prices make plant more feasible.

Fuel for Steam	Electricity Sales Prices, TR
Coal	0,055 $/kWh (Feb,2016)
Biomass	0,133 $/kWh (feed-in)
Nuclear (Akkuyu NPP)	0,123 $/kWh (feed-in)

Fuel for Steam	Steam Generation Prices, TR
Natural Gas	0,026 $/kWh (Feb,2016)
Coal (imported)	0,018 $/kWh (Feb,2016)
Biomass (straw)	0,012 $/kWh (Feb,2016)

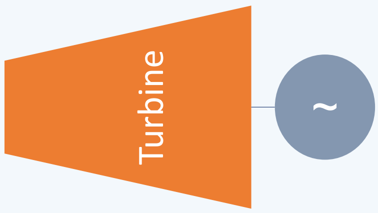

Depends on the power plant overall electricity generation efficiency, steam prices and electricity prices should be compared if there is an extraction of steam or not.

In my thesis, the fuel is municipal waste and there is fixed feed-in tariff in electricity prices so the turbine in my design will be **reaction bladed turbine & condensing type.**

Multicomponent seismic loss estimation on the North Anatolian Fault Zone (Turkey)

Fatma Nurten Sisman (f.nurtensisman@gmail.com), Aysegul Askan (aaskan@metu.edu.tr),

Shaghayegh Karimzadeh (shaghayegh.karimzadehnaghshineh@metu.edu.tr)

I. Abstract: One approach to model the high-frequency attenuation of spectral amplitudes of S-waves is to express the observed exponential decay in terms of Kappa factor. Kappa is a significant parameter used for identifying the high frequency attenuation behavior of ground motions as well as one of the key parameters for stochastic strong ground motion simulation method. Recently, it has been also used in adjusting ground motion predictions from one region to another. Currently, other than a previous study by the authors, there are no detailed studies on kappa using Turkish strong ground motion datasets. In this study, with the objective of deriving regional kappa models, we examine ground motion datasets from different regions in Turkey with varying source properties, site classes and epicentral distances. Statistical tools are used to investigate the dependency of kappa on these parameters. In addition, potential correlations between kappa and Vs30 values of the stations are also studied. Main findings of this study are regional kappa models on North Anatolian Fault zone. Finally, we also present high-frequency strong motion simulations of past events in the selected regions using the proposed kappa models. Regardless of the magnitude, source-to-site distance and local site conditions at the stations, the high-frequency spectral decay is simulated effectively.

II. Study Region: Düzce and Erzincan

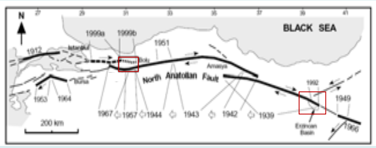

Figure 1. North Anatolian Fault Zone (NAFZ) and earthquakes along the NAFZ (Akyuz et al., 2002)

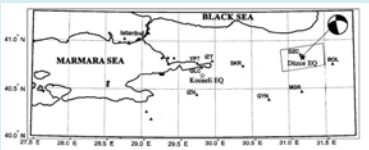

Figure 2. Study region of the Western NAFZ (Ugurhan and Askan 2010)

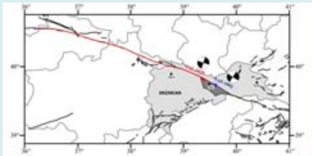

Figure 3. Study region of the Eastern. NAFZ Seismotectonics in the Erzincan region with the fault systems and the epicenters of the 1939 and 1992 events (Askan et. al. 2013)

III. Analyses for Kappa:

- We present an example for a manual pick of frequencies f_e and f_x for computing kappa from direct shear-wave spectrum in comparison with noise spectrum of the record .
- Initially we select S-wave portion of the record visually.
- We then calculate Fourier amplitude acceleration spectra with a logaritmic y-axis (Amplitude) and a linear x-axis (frequency) and select the starting frequency of the linear downward trend () (f_e) and the ending frequency of the linear downward trend (f_x).
- Consequently, we calculate the kappa factor for each three components.

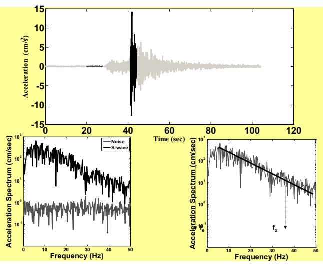

IV. Regional Kappa Models for Western NAFZ (Düzce):

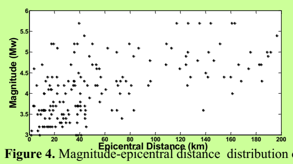

Figure 4. Magnitude-epicentral distance distribution of the dataset

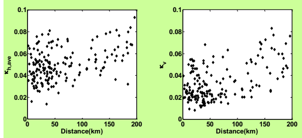

Figure 5. Variation of the (a) average horizontal and (b) vertical kappa values with epicentral distance

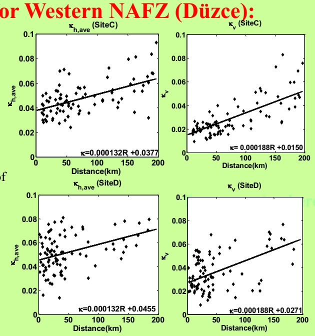

Figure 6. Variation of (left panel) and (right panel) with epicentral distance for different site classes

- Kappa values are computed from 174 records measured at 15 different strong motion stations from 142 earthquakes with magnitudes 3.0<Mw<6.0 in Northwestern Turkey.
- A linear effect of magnitude on kappa is not found statistically signficant for the database studied herein (Figure 6). The regional model is given as follows:

$$\kappa_h = 0.0377 \times Site\ C + 0.0455 \times Site\ D + 0.000132 \times R$$

$$\kappa_v = 0.0150 \times Site\ C + 0.0271 \times Site\ D + 0.000188 \times R$$

Station ID (LOCATION_CODE)	Latitude-Longitude	V_{S30} (m/s)	Site Class (NEHRP)	$\kappa_{h,0}$	$\kappa_{v,0}$
BURSA_GEMLIK_1609	40.43- 29.17	228	D	0.0414	0.0283
DUZCE_8101	40.84- 31.15	282	D	0.0527	0.0308
BOLU_1401	40.75- 31.61	294	D	0.0485	0.0303
SAKARYA_5401	40.74- 30.38	412	C	0.0387	0.0145
ISTANBUL_3401	41.06 -29.01	595	C	0.0342	0.0133

V. Regional Kappa Models for Eastern NAFZ (Erzincan):

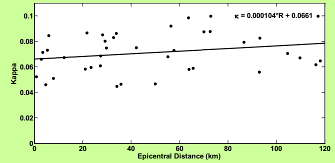

Figure 7. Regional distance-dependency of kappa computed at stations ERC, REF and TER (Askan et. al. 2013)

- The dataset used for the Eastern NAFZ kappa model consists of 40 records measured at the three stations available.
- We note that the original database had slightly more data than those employed herein however, only the records with clear S-wave arrivals and no signal-to-noise problems are selected for reliable kappa computations
- Single model for the C and D type soils: $\kappa = 0.0661 + 0.000104\,R$

Station	Latitude (^{0}N)	Longitude (^{0}E)	Vs30 (m/s)	Site Class (NEHRP)
ERZINCAN-2401	39.752	39.487	314	D
REFAHIYE-2403	39.899	38.768	433	C
TERCAN-2405	39.777	40.391	320	D

VI. Use of Regional Kappa Models in Ground Motion Simulations:

Modeling in Erzincan Region	Event 1: 13/03/1992 Erzincan Earthquake (Mw=6.6)
Parameter	**Value**
Epicenter Location	39°42.3 N, 39°35.2 E
Fault orientation	Strike: 125° Dip: 90°
Fault dimensions	25 × 9 km
Hypocenter depth	9 km
Stress drop	80 bars
Quality factor	$122f^{0.68}$
Duration model	T_0+0.05R
Geometric spreading	$R^{-1.1}$, $R \leq 25$ km $R^{-0.5}$, $R > 25$ km
Windowing function	Saragoni-Hart
Site Amplifications	Local model at each station
Kappa	Regional kappa model (k_0=0.066)

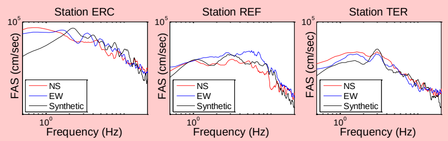

Figure 8. Comparison of the simulated and observed Fourier amplitude spectra at selected stations for 1992 Erzincan earthquake (Mw=6.6)

Modeling in Düzce Region	Event 1: 12/11/1999 Gölyaka Earthquake (Mw=5.2)	Event 2: 12/11/1999 Düzce Earthquake (Mw=7.1)
Parameter	**Value**	**Value**
Epicenter Location	40.75 N-31.1 E	40.79 N-31.21 E
Fault orientation	Strike: 270° Dip: 90°	Strike: 264° Dip: 64°
Fault dimensions	4 × 4 km	65 × 25 km
Hypocenter depth	9.3 km	12.5 km
Stress drop	30 bars	100 bars
Quality factor	$88f^{0.9}$	
Duration model	T_0+0.05R	
Geometric spreading	R^{-1}, $R \leq 30$ km $R^{-0.4}$, $30 < R \leq 60$ km $R^{-0.6}$, $60 < R \leq 90$ km $R^{-0.8}$, $90 < R \leq 100$ km $R^{-0.5}$, $R > 100$ km	
Windowing function	Saragoni-Hart	
Site Amplifications	Locally-derived empirical HVSR functions for DUZCE and BOLU stations , generic site amplifications for ISTANBUL and SAKARYA stations	
Kappa	Single Station k_0 values obtained according to the regional model proposed	

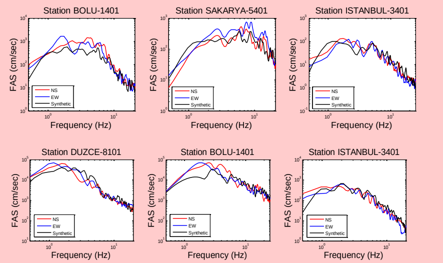

Figure 9 .Comparison of simulated and observed Fourier amplitude spectra at selected stations for the 1999 Gölyaka earthquake (Mw=5.2) (top panel) and 1999 Düzce earthquake (Mw=7.1)

VII. Conclusions:

- Regional kappa models on Eastern as well as Western NAFZ are obtained.
- Kappa models are tested in stochastic finite fault simulations of selected earthquakes occured in the regions.
- Regardless of the magnitude, source to site distance and local site conditions at the stations, the high frequency spectral decay is simulated effectively.
- The proposed kappa models can be used to represent the near-surface high frequency spectral decay in future ground motion simulations in the region.

VIII. References:

Askan, A., Sisman, F.N., and Ugurhan, B. (2013). Stochastic strong ground motion simulations in sparsely-monitored regions: A validation and sensitivity study on the 13 March 1992 Erzincan (Turkey) earthquake, Soil Dynamics and Earthquake Engineering, 55, 170-181.

Askan, A., Sisman F.N. And Pekcan, O. (2014). A Regional Near-Surface High Frequency Spectral Attenuation (Kappa) Model for Northwestern Turkey.Soil Dynamics and Earthquake Enginnering, Volume 65,Pages 113-125

Ugurhan, B., Askan, A., (2010), Stochastic Strong Ground Motion Simulation of the 12 November 1999 Düzce (Turkey) Earthquake Using a Dynamic Corner Frequency Approach, Bull. Seism. Soc. Am. 100, 1498-1512.